Journal of Mechanical Design. Received February 01, 2023;
Accepted manuscript posted October 21, 2023. doi:10.1115/1.4063966
Copyright © 2023 by ASME

Check for updates

Design space exploration and evaluation using margin-based trade-offs

Khalil Al Handawi
Mechanical Engineering
McGill University
Montréal, Canada
khalil.alhandawi@mail.mcgill.ca

Arindam Brahma*
Industrial and Materials Science
Chalmers University of Technology
Göteborg, Sweden
brahma@chalmers.se

David C Wynn
Department of Mechanical and
Mechatronics Engineering
University of Auckland
Auckland, New Zealand
d.wynn@auckland.ac.nz

Michael Kokkolaras
Mechanical Engineering
McGill University
Montréal, Canada
michael.kokkolaras@mcgill.ca

Ola Isaksson
Industrial and Materials Science
Chalmers University of Technology
Göteborg, Sweden
ola.isaksson@chalmers.se

Accepted Manuscript Not Copyedited

Design space exploration and margin analysis can inform critical decisions early in engineering design, helping to handle the uncertainties of early design while ensuring design performance. In practice, the complexity of many products makes such decision-making challenging. This paper addresses the challenge with a new design framework that relies on the margin value method to evaluate sets of concepts that are combinatorially generated from an enhanced function-means tree. The basis for concept comparison is the margin value in each design alternative. The margin value method is expanded to address a broad class of design problems by using surrogate models and novel metrics for evaluating different conceptual alternatives. Visualization tools are introduced to support the evaluations. The efficacy of the framework is demonstrated using the design of a structural aero-engine component involving simulation models and uncertain load specifications. Overall, this paper shows how design concepts can be compared objectively and distilled to a set of alternatives that would retain their values throughout product development.

Keywords: Design space exploration, Design margins, Margin value method, Set-based design, Design under uncertainty, Parallel coordinates

*Address all correspondence to this author.

1 Introduction

Design space exploration for complex engineering products can be challenging, especially in the early design phases that are subject to many uncertainties [1]. Design complexity and the time and cost constraints emanating from competitive market needs often require critical decisions to be undertaken very early in the design process. The standard practice for design within frameworks such as stage-gate and Vee models is to create and iterate on individual subsystem designs until they integrate to fulfil the requirements, attempting to control the iterations through careful upfront definitions of interfaces [2]. An alternative is offered by set-based concurrent engineering (SBCE), which advocates focused learning about a design's feasibility at a very early stage [3]. Initially, multiple feasible design solutions are created; solutions are gradually eliminated throughout the design process due to integration difficulties for combinations of sub-solutions or any other reason which may become apparent as designs are elaborated [4]. One advantage of SBCE is to reduce late design iterations, which should accelerate product development.

The need for faster product development has also led to technology-driven approaches such as generative design [5], which aim to accelerate the exploration of design spaces and convergence to an optimum solution. The growth in popu-

 Copyright © by ASME

Downloaded from http://asmedigitalcollection.asme.org/mechanicaldesign/article-pdf/doi/10.1115/1.4063966/7056417/md-23-1056.pdf by McGill University user on 06 November 2023

Journal of Mechanical Design. Received February 01, 2023;
Accepted manuscript posted October 21, 2023. doi:10.1115/1.4063966
Copyright © 2023 by ASME

larity of these methods has been aided by rapidly increasing computing power [6] and new manufacturing technologies which can realise topologies that could not previously be manufactured using traditional methods [7]. While a multitude of generative design approaches exist [8], they typically do not relate product-level information to the design choices or parameters [9], which makes them challenging to use when novel design functionalities are to be integrated into pre-existing designs [10]. Some methods address this gap by using the functional domain to aid exploration, such as Müller et al.'s object model for function and geometry (OMFG) [10, 11]—these produce a large number of concepts combinatorially, from which feasible designs need to be extracted. But they do not provide support to evaluate or rank the generated concepts. This is needed to arrive at smaller, more manageable sets of solutions that can undergo simulations such as finite element analysis (FEA) to compare their performance levels more comprehensively.

In this paper, we introduce a new framework for design space exploration (DSE) which enables the generation and early assessment of candidate designs, addressing the aforementioned limitations with a view to accelerating the overall design process. The framework consists of two parts. The first part involves generating a large number of feasible solutions automatically. It builds upon the work of Müller et al. to find feasible solutions from a functionally generated solution set. Considering the feasibility reduces a large number of possible concepts generated combinatorially to a smaller number. The second part of the framework involves ranking the generated concepts based on their values, calculated using a design margins metric based on the work of Brahma and Wynn [12]. In this work, the value is based on the trade-off between desirable and undesirable effects of margins in a candidate design. While some of the margins can be used to absorb changes later in the design's lifecycle, thereby increasing its value, they also have undesirable effects on the design's performance, such as increasing weight.

The specific contributions of this paper can be summarised as follows.

1. An approach is introduced to couple function-based combinatorial generation of designs to a method which can locate and analyse margins in a design.
2. A new metric is introduced to measure designs' values in terms of excess margins. This enables the ranking of the combinatorially generated design solutions.
3. The above two contributions are combined into a new design space exploration approach for early design phases.

Next, Section 2 discusses existing literature followed by the identified gaps. This is followed by details on the method development in Section 3, explained with an illustrative example in Section 4. The example illustrates the application of the method in a simplified but realistic industry-based design case. The paper ends with a discussion and conclusion in Sections 5 and 6, respectively.

2 Background

Some researchers have argued that the traditional methods of design are inherently incomplete because they do not explore all the possibilities [9, 11, 13, 14]. In concept design, engineers initially work with partial and abstract descriptions of their designs while gradually evolving them to include measurable criteria that are dealt with only in the later design stages. This drives designers in early stages to focus only on a restricted range of performance criteria while pushing comprehensive assessments to a later stage [15]. Given that the impacts of design changes increase significantly as the design moves through the stages [16, 17, 18], the design process would likely be more efficient if more comprehensive assessments were done much earlier. Further, early identification and elimination of solutions which are likely to fail at later design stages can lead to a leaner design process because resources can be concentrated on a select few solutions [15]. Similar principles can also be found in design models such as SBCE, which was first developed and observed in Toyota [19, 4]. While researchers agree on the benefits of early assessment of designs, some argue that exploring spaces of parameters is not enough for an effective DSE; requirements must also be taken into account [10, 11].

2.1 Approaches to design space exploration

Design space exploration (DSE) broadly refers to the systematic process of developing and evaluating candidate designs within a design space [13]. Functional modeling has been used to support many engineering design contexts, including DSE. For example, Mokhtarian et al. proposed an approach called dimensional analysis conceptual model (DACM), in which they extend function models to build physics-based reasoning models of products [20]. Based on the function-behavior-structure (FBS) modeling approach of Gero and Kannengiesser, DACM aims to establish a connection from the parametric domain, i.e., the design parameters of a product, to the functional domain using a variation of the bond graph representation technique [21]. The method generates causal graphs between variables and computes behavioural laws between variables considering design objectives. This can be used to identify contradictions, i.e., situations where a design variable may need to be increased and decreased simultaneously to satisfy a set of design objectives. Mokhtarian et al. propose ways to improve the design by specifically addressing these contradictions. However, they do not indicate how the resulting design solutions could be modeled. Further, since the approach is aimed at an incremental design context, the development of new concepts or the approach's application in the early design phases may be difficult.

Wang et al. proposed an ontology-based method which uses a template-based approach for DSE [14]. The pro-

Accepted Manuscript Not Copyedited
Downloaded from http://asmedigitalcollection.asme.org/mechanicaldesign/article-pdf/doi/10.1115/1.4063966/7056417/md-23-1056.pdf by McGill University user on 06 November 2023

Journal of Mechanical Design, 0000, 0 (0): 0000000, 0 pages
Accepted manuscript posted October 21, 2023. doi:10.1115/1.4063966
Copyright © 2023 by ASME

posed method involves the development of a mathematical model based on the identified requirements, objectives, decisions, and other related variables. The mathematical model also involves the identification of the significant design parameters such as the control, noise, and response factors, their corresponding ranges and relationships. They apply the "compromise decision support problem" method to this model to generate a range of solutions, which are then used to explore the design space. Elicitation of the design solution in terms of ranges instead of a point solution facilitates adjustments throughout the design stages. Another approach was presented by e Costa et al. aimed at customer participation in DSE [22]. Two interlinked software modules are presented. One of the modules is used by the designer to parametrically model a product, whereas the other is used by the end-users to explore the design space. An interpolation-based approach is used. Both these approaches, however, are limited to the parametric domain and analysis of higher-level domains, such as functions, is not possible.

Commercial software solutions for DSE also exist. Koch et al., for instance, introduced a software platform called iSIGHT^{TM} which integrates multiple optimization algorithms, design of experiments (DOE) methods, approximation techniques, and quality engineering methods under one software platform for DSE [23]. While enabling the use of many standardised methods and interfacing with external simulation tools, similar to the previous approach discussed, iSIGHT^{TM} is also limited to parameters and does not account for the functional domain.

Müller et al. explored the possibility of exploring design spaces using the functional domain. They show that using the functional domain in the exploration process widens the scope of exploration and therefore can elicit solutions with novel characteristics [11]. The approach is to connect the product's design rationale using an enhanced function-means (EF-M) model which consists of pairs of functional requirements, representing the mandate of the design, and design solutions, representing the various means of satisfying those requirements. The modeled information is used to generate a feasible solution space. Furthermore, the model also allows for analyses in the functional domain—this makes it possible to view the design from both high and low-level perspectives which is advantageous when design changes occur [24]. The authors also point out the effort needed to combinatorially generate concepts and explain how the growth in the number of possible combinations is usually exponential. Analysing such a large number of concepts and making trade-offs between them is not just laborious but virtually impossible. Further, once model parameters are formulated, the scope for parametric variation within each concept is also large in most cases. This makes trade-off studies even more challenging.

2.2 Flexibility, robustness, and margins in candidate designs

SBCE suggests that flexibility in early design is one of the key success criteria in making the design process more efficient [4]. In the context of SBCE, flexibility is implemented by initially setting up broad specifications and loose constraints, which can be narrowed down as details emerge [25]. Another way to look at flexibility is through Upton's definition as *"the ability to change or react with little penalty in time, effort, cost or performance"* [25, 26] or as the ability to respond to changes in requirements [27]. Apart from flexibility, adaptability and robustness are also commonly used concepts in the management of uncertainties, including those occurring in early design [28, 29]. Robust design, first developed by [30], is defined in terms of achieving a fixed behaviour over a range of external influences [31]. The concepts surrounding robust design were initially proposed in the context of making designs insensitive to noises from manufacturing processes [32] and have since been extended to other uncertainties. These include uncertainties in both the design and process domains [33, 34]. To provide one relevant example of a robust design approach, Chang et al. draw from Taguchi and Clausing's parameter design concepts in a method to make designs more robust to changes [35, 30]. Their focus is on changes that potentially arise due to the collaborative nature of design in a concurrent engineering setting. According to Chang et al., the primary reason for such changes is that decisions are made simultaneously by separate teams working on various parts of the design. Optimization techniques are used to increase a design's robustness while treating possible variations as "conceptual noise".

Another method to make a candidate design insensitive to uncertainty and future change is the use of margins. Margins appear throughout the product development process in different forms. Some are included deliberately to mitigate uncertainties. For example, margins may be built into requirements to address regulatory, safety or life requirements. Margins may also be added to make a product reliable [36]. Input specifications can hardly be predicted with absolute certainty and required margins are sensitive to such variability [37]. Engineers may also add margins to parameters in product designs [38, 39], which enables the absorption of changes in product specifications [12] and can allow upgradability [40]. Inadvertent inclusion of margins may be a result of suboptimal design or using off-the-shelf components. Regardless of the reasons for inclusion, margin can lead to over-design [41]. In other words, adding margin may make the design process efficient, since less rework will be required due to changes in uncertain specifications, but the design itself may become more inefficient, wasteful, and over-designed, leading to performance deterioration [38]. Overall, therefore, it is important to trade off the benefits of margin, such as flexibility or change absorption capability, against the potential undesirable impact it may entail [12]. This requires quantitative margin analysis.

Accepted Manuscript Not Copyedited
Downloaded from http://asmedigitalcollection.asme.org/mechanicaldesign/article-pdf/doi/10.1115/1.4063966/7056417/md-23-1056.pdf by McGill University user on 06 November 2023

Journal of Mechanical Design, Received February 01, 2023;
Accepted manuscript posted October 21, 2023. doi:10.1115/1.4063966
Copyright © 2023 by ASME

Methods to quantify margins have been investigated by many researchers. Traditionally Factor of safety (FoS) has been one of the most well-known types of margin, with many methods and approaches available. However, approaches to quantify FoS generally tend to be context-specific, such as in the context of bridge design [42], hull design [43], etc. Tilstra et al. provide guidelines for suitable use of margins to make designs more flexible against future changes arising from product evolution [44]. Tan et al. further extend this by using Multi-disciplinary optimization (MDO) to trade off performance and design margins while aiming to increase the robustness of the designs [45]. In another method, functional decomposition is used to model margins and quantify them [46]. Deriving from the concept of design space, Guenov et al. proposed the use of an "explicit margin space", which allows the study of the allowable limits of margins on certain parameters when margins are allocated on certain other parameters [40]. In another stream of work, the Change Prediction Method by Clarkson et al. is applied to identify significant margins in design [27, 47]. They hypothesize that low change propagation probability indicates high levels of margin and vice-versa. While many of these methods enable the quantification of margin, they do not provide an aggregating metric which can be used to assign a value to a design, which is needed to meet the objectives of this article. One of the primary challenges is to compare margins in different forms. For example, some margins in a design may be specified in Newtons, while others may take the form of differences in material strengths. A method that does aggregate different forms of margin is Brahma and Wynn's margin value method (MVM), which can be used to identify, localize, and size margins in a design [12]. In this method, the undesirable effect of margin can be traded-off against the design's flexibility against changes in specification parameters. To do this, Brahma and Wynn propose two metrics of change absorption capability (CAC) and impact on performance (IoP), formulated such that the margins become comparable. The metrics provide the opportunity to be aggregated, and therefore be used as a proxy for the value of the design in terms of flexibility and adverse IoP due to excess margin. A similar trade-off between capability and performance was observed by Al Handawi et al. for a single functional requirement-design solution pair [48].

2.3 Overview of the MVM

The MVM developed by Brahma and Wynn analyzes and evaluates design alternatives at the preliminary design stage in terms of the value of design margins by considering the context of the desirable aspects of margin such as change absorption potential and the undesirable effect margins have on the performance of the system. Change absorption is quantified by incrementally varying the design requirements (e.g, the load to be supported by a structural bracket) and calculating the maximum amount of deviation in the requirement that can be supported by the current design. The impact of margins on the product's performance is the loss in performance (e.g., the weight of the bracket) relative to a hypothetical design with zero margins (e.g., a lean bracket with excess geometry shaved off), denoted as the threshold design. The following is a brief overview of the steps involved in MVM. Detailed steps and a pseudo-algorithmic formulation of the method are presented in the supplemental material (Algorithm 1).

1. Construct a margin analysis network (MAN): This is a network representing the flow of dependencies that connect the input (design specification) parameters to the design performance parameters, via calculations, intermediate parameters and design decisions.
2. Margin Value Analysis: The margin value analysis consists of calculating three metrics:
   (a) Local excess margin: Each decision in the MAN is accompanied by excess margin due to a discrepancy between the capability resulting from that decision (defined as the decided value) and what is required to achieve its function (defined as the target threshold). This excess is defined at a margin node and is represented using a vector $\mathbf{e} \in \mathbb{R}^n$, where n is the number of margin nodes.
   (b) Impact on performance (IoP): Indicates the deteriorating effect of each margin node on each performance parameter represented as a matrix $\mathbf{I} \in \mathbb{R}^{n \times n_{\text{perfs}}}$, where n_{perfs} is the number of performance parameters. It can be thought of as a measure of the undesirable byproduct of excess margin on the design's performance.
   (c) Change absorption capability (CAC): Relates to the amount of variation in input specifications each margin node can absorb before design change is required. CAC is represented as a matrix $\mathbf{A} \in \mathbb{R}^{n \times n_{\text{specs}}}$, where n_{specs} is the number of input specifications.
3. Margin value plot (MVP): The two metrics of IoP and the CAC can then be plotted which shows the relative importance of every margin node in terms of their absorption capability and the deteriorating effect on the performance of the system.

As described by Brahma and Wynn, the method was originally developed for an incremental design context, where a design exists and improvements are made by making adjustments to it [12]. The method was not intended to be used in DSE, and its original form can only be applied to one design at a time. This paper, in contrast, addresses situations in which designs do not pre-exist and are generated through a DSE approach based on functional modeling. Further, the margin value method focuses extensively on off-the-shelf components such as motors, bearings, etc. In contrast, the application context of this paper is a single component, which cannot be disassembled once manufactured.

2.4 Summary

While there are a number of methods for design space

Accepted Manuscript Not Copyedited
Downloaded from http://asmedigitalcollection.asme.org/mechanicaldesign/article-pdf/doi/10.1115/1.4063966/7056417/md-23-1056.pdf by McGill University user on 06 November 2023

Journal of Mechanical Design [DOI: 10.1115/1.4063966]
Accepted manuscript posted October 21, 2023. doi:10.1115/1.4063966
Copyright © 2023 by ASME

exploration, they have certain limitations. Some DSE methods are limited to the incremental design context, while others are limited to the parametric domain. Methods which consider the functional domain to allow broader exploration do not indicate how the generated concepts can be filtered considering trade-offs to produce a more manageable set of feasible solutions. One way of addressing this challenge is by analysing margins in each solution to determine their values in terms of their abilities to absorb uncertainties and hence retain the flexibility required for future development. In particular, the margin value method shows that, while substantial margins may be desirable from an uncertainty absorption point of view, they make a design inefficient and have a deteriorating impact on its performance. This trade-off can provide a basis to assess the value or 'goodness' of feasible designs generated in DSE. Keeping these points in mind and seeking to address some limitations of existing DSE approaches, the following sections present a framework to extract and rank feasible design solutions from a functionally generated solution set based on their margin values.

3 A DSE approach based on functionally-generated design concepts and MVM

In overview and prior to a detailed worked example, this section presents the process steps for the developed DSE approach (shown in Figure 1). The first two steps correspond to the functional modeling of the design and the subsequent combinatorial generation of feasible design solutions [11]. Steps 3a and 4–6a describe the MVM in the context of DSE. Step 4 describes how the infeasible designs are distinguished to create the feasible design set. Step 6b relates to the new metric required to rank the concepts. Finally, in Step 7, the solutions are ranked based on their values.

Step 1: Construct an EF-M tree similar to Figure 1a to represent multiple means that could be used to realize each required function of the design.

Step 2: Generate a set of possible combinations of the means captured in the EF-M tree to produce concepts categorized by their functional means. For example, the tree in Figure 1a depicts two possible concepts based on a combination of design solutions $\{\mathrm{DS}_1, \mathrm{DS}_2^A, \mathrm{DS}_3\}$ and $\{\mathrm{DS}_1, \mathrm{DS}_2^B, \mathrm{DS}_3\}$, respectively.

Step 3a: Follow the steps described in ref. [12] to create a MAN such as the one shown in Figure 1b for each category of concepts that share the same functional means. For example, two MANs will need to be created for the two categories $\{\mathrm{DS}_1, \mathrm{DS}_2^A, \mathrm{DS}_3\}$ and $\{\mathrm{DS}_1, \mathrm{DS}_2^B, \mathrm{DS}_3\}$ identified in step 2. Hyperlinks between the EF-M tree and each MAN model relationships between functional requirements in the EF-M tree with input specifications in the MAN (hyperlink 1 in Figures 1a and 1b) and, design solutions with decision nodes (hyperlinks 2 and 3 in Figure 1a and 1b).

Step 3b: Use each MAN to enumerate more conceptual alternatives by varying the decisions in MAN (the orange diamonds) to exhaustively enumerate all possible concepts.

Step 4: Evaluate the calculations in the MANs, make decisions, and quantify excess margin. We denote the models describing relationships between input specifications, decision nodes, excess margins, and performance parameters as *behaviour models*. Surrogate models may be used as behaviour models since they scale well with designs featuring a large number of margin nodes, input specifications, and performance parameters. In this paper, an open-source surrogate modeling toolbox was used for all surrogate models [49]. Only designs with positive excess margins ($\mathbf{e} \geq \mathbf{0}$) are considered for subsequent steps. This set of designs is the feasible set. Furthermore, uncertainty surrounding input specifications can be modeled using probability density functions (PDFs). Input specifications can be repeatedly sampled and the frequency distribution of excess margins and other MVM metrics estimated [50, 48]. In the case of probabilistic specifications, *reliability* can be calculated as the area under the frequency distribution of excess where excess margins exceed zero [51]. Feasible designs with non-zero reliability are considered in the following steps.

Step 5: Calculate the MVM metrics, IoP and CAC.

Step 6: Plot CAC and IoP (or their means in case of probabilistic specifications) on a MVP. We use the MVP to compare the design concepts enumerated by the EF-M. Brahma and Wynn explain that margin nodes offer maximum value when their CAC is high while their IoP is low. In MVM, both these metrics are produced as arrays, where the dimension of the arrays corresponds to the number of margin nodes in the design. Since in DSE the number and nature of margin nodes may not be comparable, using the metrics in their original form is not possible. To counter this, a new metric is introduced which captures an aggregate value of the CAC and IoP, representing the design's value based on its margins. This not only helps in comparing all the concepts on a single scale, but it also enables the selection of promising concepts from the set of generated concepts. The value metric can be used to assess the proximity of each margin node to this region of the MVP. Figure 1c shows an example of the MVP with a single design plotted. The neutral line (dashed line) is constructed by defining $I_{\min}, A_{\min}$ and $I_{\max}, A_{\max}$, representing the minimum and maximum values for impact and absorption, respectively. The value v_{design} of a design given by coordinates (I, A) is calculated using Equation (1) as

$$v_{\text{design}} = \frac{\left\| \begin{bmatrix} I_{\max} - I_{\min} \\ A_{\max} - A_{\min} \end{bmatrix} \times \begin{bmatrix} I - I_{\min} \\ A - A_{\min} \end{bmatrix} \right\|}{\left\| \begin{matrix} I_{\max} - I_{\min} \\ A_{\max} - A_{\min} \end{matrix} \right\|}, \tag{1}$$

where I and A are calculated by averaging the elements across rows of matrices $\mathbf{A}$ and $\mathbf{I}$, respectively (see Equation S.8 and Brahma and Wynn [12]). The rationale behind the value metric in Equation 1 is that v_{design} increases the further the coordinates (I, A) are from the neutral line, due to their proximity to the high-value region in Figure 1(c).

Downloaded from http://asmedigitalcollection.asme.org/mechanicaldesign/article-pdf/doi/10.1115/1.4063966/7056417/md-23-1056.pdf by McGill University user on 06 November 2023
Accepted Manuscript not copyedited

Journal of Mechanical Design. Received February 01, 2023;
Accepted manuscript posted October 21, 2023. doi:10.1115/1.4063966
Copyright © 2023 by ASME

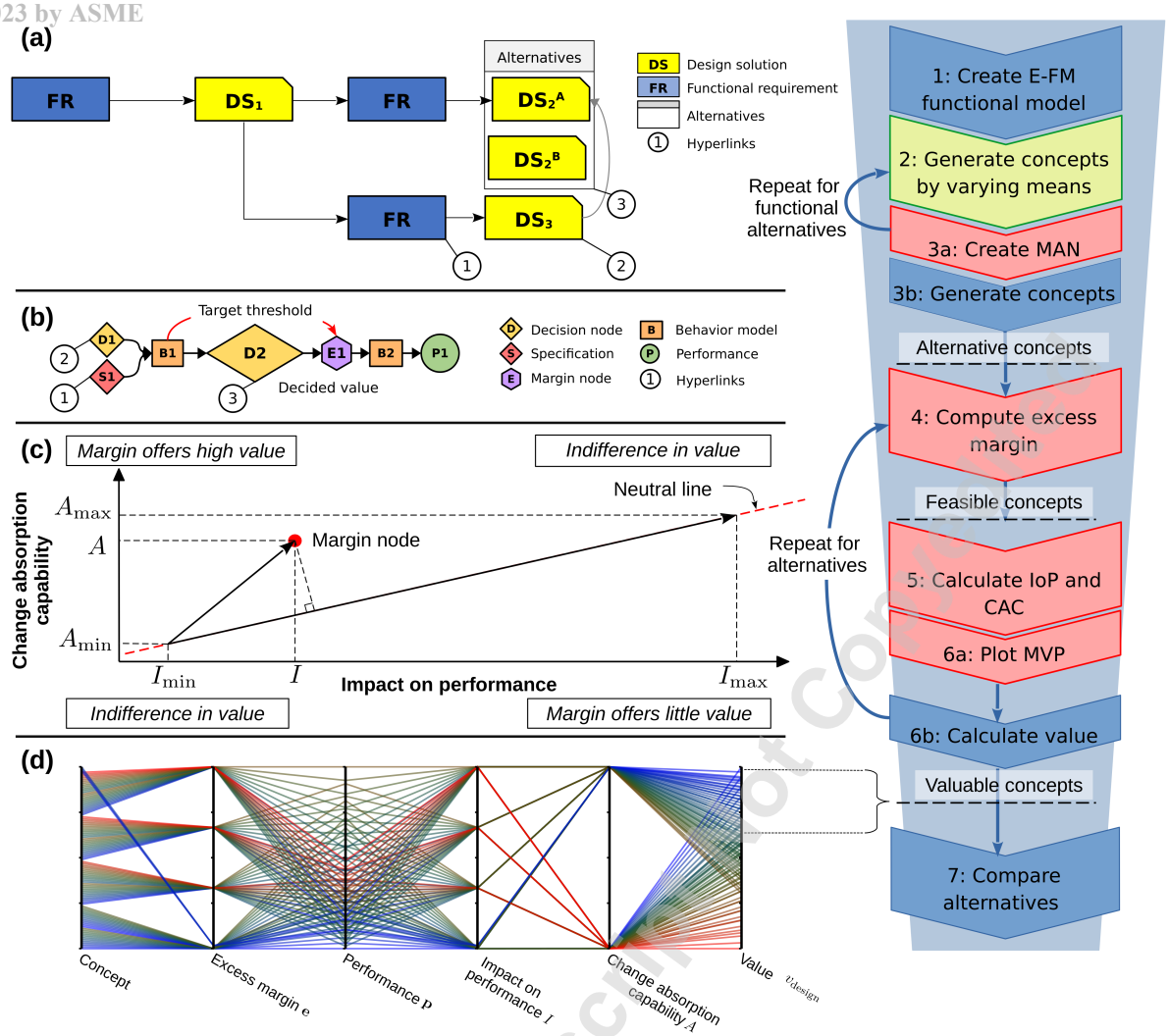

Fig. 1: Process model for generating and evaluating conceptual design alternatives in terms of excess margin value. The blue chevrons represent the components of the methodology proposed in this paper. The red chevrons represent work done by Brahma and Wynn [12]. The green chevron represents Müller et al.'s work [11].

Step 7: Repeat steps 4-6 until all the conceptual alternatives are filtered by feasibility and then evaluated. The MVM parameters, such as excess margin, performance, and value, are compared on a parallel coordinates plot (PCP). A filter can be used to eliminate alternatives that offer little value. An example is shown in Figure 1d. The top-performing concepts are retained for further analysis and development.

4 Illustrative example

Aerospace parts undergo long product development cycles involving a lot of decisions during conceptual design. These decisions involve excess margins that may affect the performance of the aircraft. Since the performance of aerospace products is very sensitive to excess margins, we will present an example in which an aeroengine part is designed using the approach presented in Section 3.

The turbine rear structure (TRS) is a static structure located aft of the turbine and before the exhaust nozzle [52]. The location of the TRS within an aeroengine assembly is shown in the supplemental material, Figure S.Ia.

We focus on the design of the struts and shroud which provide structural support to the TRS under thermomechanical loads as a result of temperature gradients across the annulus of the TRS due to hot exhaust gases as shown in Figure 2b. They also support bearing loads applied on the hub as shown in Figure 2d. The following section shows how multiple concepts for the struts can be enumerated and analyzed using the MVM.

4.1 Step 1: Functional modeling

A functional model using EF-M trees is built for the strut subsystem of the TRS as shown in Figure 3. The functional requirements (blue boxes) represent the thermal and bearing loads shown in Figure 2. These requirements and corresponding design solutions (yellow boxes) are described in Table 1.

Downloaded from http://asmedigitalcollection.asme.org/mechanicaldesign/article-pdf/doi/10.1115/1.4063966/7056417/md-23-1056.pdf by McGill University user on 06 November 2023

Journal of Mechanical Design ... 2023;
Accepted manuscript posted October 21, 2023. doi:10.1115/1.4063966
Copyright © 2023 by ASME

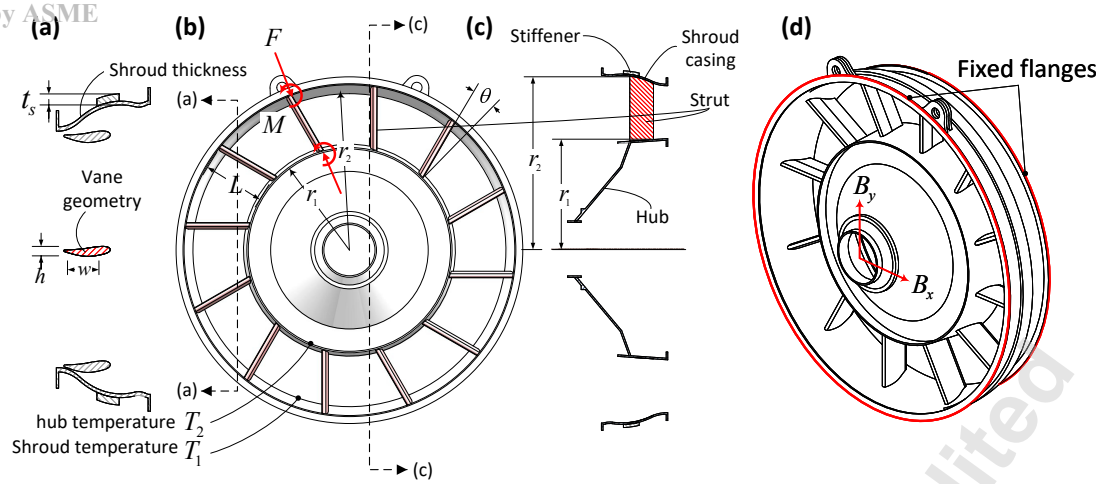

Fig. 2: computer-aided design model of the turbine rear structure (TRS) used in this study. (a) Cross-sectional view of the turbine rear structure (TRS) along struts (showing vane geometry), (b) Front view of the turbine rear structure (TRS), (c) cross-sectional view of the turbine rear structure (TRS) showing details of the hub design, and (d) application of bearing loads on the turbine rear structure (TRS).

Table 1: Summary of interactions between EF-M tree and MAN of the strut example.

Hyperlink	Solution	Description	Parameters	Units	Design choices	
1	DS1	Vane cross-section geometry	w	mm	60, 70, 80, 90, 100, 110, 120	
			h	mm	14, 16, 18, 20	
2	DS2	Material selection	material	-	Steel, Inconel, Titanium	
3	DS3	Strut lean geometry	θ	°	0, 10, 20, 30, 40, 50	
4	DS4	Multiple struts	n_{struts}	-	6, 8, 10, $\cdots$, 30	
5	DS5	Shroud design			polygonal, circumferential	
6	DS6	Shroud thickness	t_s	mm	2, 2.5, 3, $\cdots$, 8.0	
Hyperlink	**Requirement**	**Description**	**Parameters**	**Units**	**Nominal value**	**PDF**
7	FR1	Must not deform shroud and hub	T_1	°C	450	$\mathcal{U}(350,550)$
			T_2	°C	425	$\mathcal{U}(325,525)$
8	FR2	Transmit bearing loads	B_x	N	100	$\mathcal{U}(95,105)$
			B_y	N	100	$\mathcal{U}(95,105)$

4.2 Step 2: concept generation and embodiment

A number of conceptual alternatives can be enumerated from the EF-M tree. We demonstrate this using a limited example with 8 conceptual alternatives (shown in Table 2) and an extended example with 13,104 alternatives.

There are two possible choices for each of the strut geometry, vane cross-section, and shroud design—as shown in Table 2. As a result, eight combinations of three design solutions can be formed for the limited example.

For the extended example, Table 1 lists 7×4 choices for the vane cross-section, 3 choices for the material, 6 choices for the strut geometry, and 13 choices for the number of struts, and 2 choices for the shroud design yielding a total of 13,104 alternatives. The shroud thickness is chosen such that excess associated with it is minimized for every design alternative.

4.3 Steps 3 and 4: Construction of the MAN and calculation of excess margin

Figure 4 shows a MAN for alternatives with circumferential shrouds. Input specifications (red diamonds) and design decisions (orange diamonds) which interact with the EF-M are defined in Table 3. Fixed (white diamonds), intermediate, and performance parameters (green circles) which do not interact with the EF-M directly are also defined in Table 3. A second MAN for polygonal shroud concepts and its corresponding parameters and models are explained in the supplemental material, Section S.III and is shown in Figure S.III. All the behaviour models (orange boxes) and their detailed derivations are provided in the supplemental material, Section S.III through Section S.V and Tables S.III and S.I for the circumferential and polygonal shroud configurations, respectively.

For both MANs, the height h and lean angle θ decisions are varied according to the design alternative being evaluated (see Table 2) for the limited example.

4.4 Step 5: Computation of IoP and CAC

We first model the uncertainty in input specifications using uniform PDFs defined in Table 1. In practice, these PDFs are often possible to estimate based on knowledge of the design situation and previous experience. 1,000 samples were drawn (8 × 1,000) for the limited example and 100 samples (13,104 × 100) for the extended example. For each sample, the excess margins are allocated by selecting a material, vane cross-section width w, number of struts n_{struts},

Accepted Manuscript Not Copyedited
Downloaded from http://asmedigitalcollection.asme.org/mechanicaldesign/article-pdf/doi/10.1115/1.4063966/7056417/md-23-1056.pdf by McGill University user on 06 November 2023

Journal of Mechanical Design, Accepted manuscript posted October 21, 2023. doi:10.1115/1.4063966
Copyright © 2023 by ASME

Table 2: Alternative conceptual designs for limited example.

Alternative	Design Solution	1A	1B	1C	1D	2A	2B	2C	2D
MAN		Figure S.III				Figure 4			
Strut geometry	Leaned $\theta = 30^o$		✓		✓		✓		✓
	Upright $\theta = 0^o$	✓		✓		✓		✓	
Vane cross-section	Thick $h = 17$ mm	✓			✓	✓			✓
	Slim $h = 15$ mm		✓	✓			✓	✓	
Shroud design	Polygonal	✓	✓	✓	✓				
	Circumferential					✓	✓	✓	✓

: Leaned struts, thick vanes, polygonal shroud : Upright struts, slim vanes, circumferential shroud

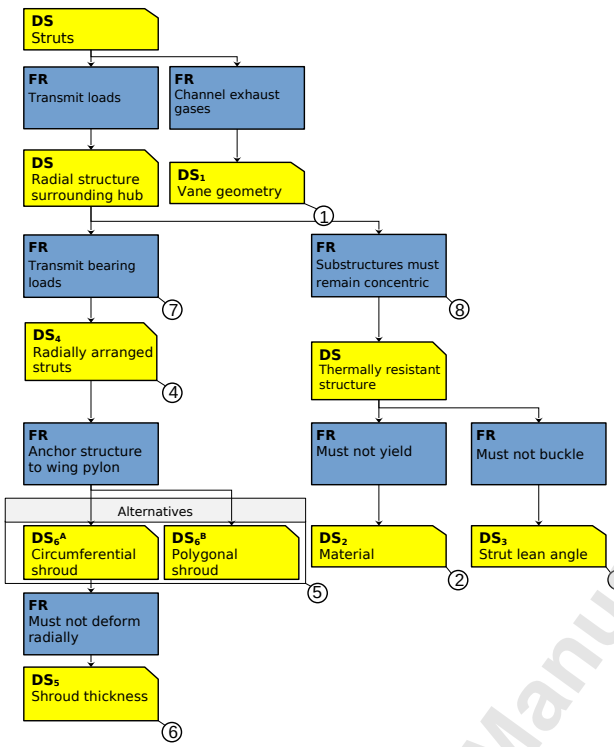

Fig. 3: Models of the the strut of the TRS showing the EF-M tree. The small numbered circles are hyperlinks showing how functions and means relate to nodes on the MAN in Figure 4.

and shroud thickness t_s from the available choices in Table 1 such that excess is minimized but remains positive to maintain design feasibility. The material choices (steel, Inconel, and titanium) in the table involve other manufacturing considerations in practice, but for simplicity and demonstration purposes, they are considered interchangeable in this paper. We denote this margin allocation strategy as the *minimum excess strategy*. We perform the MVM calculations that follow for steps 5 and 6 for each sample (Sections 4.4 and 4.5).

The MVM was then used to compute the IoP and CAC in steps 5 and 6 for each feasible alternative and sample (Sections 4.4 and 4.5). All eight alternatives were feasible for the limited example, while a fraction of the 13,104 alternatives remained feasible for the extended example.

Table 3: EF-M independent parameters of the circumferential concept MAN (see Figure 4).

Symbol	Units	Description
Fixed parameters		
E	GPa	Young's modulus
α	$^oC^{-1}$	Thermal expansion coefficient
r_1	mm	Radius of the hub
r_2	mm	Radius of the shroud
K		Column effective length factor
T_{sink}	^oC	Ambient temperature
$w_{nominal}$	mm	Nominal buckling width
w_s	mm	Shroud width
Intermediate parameters		
σ'_y	MPa	Yield strength
F'	N	Axial load
w'	mm	Cross-section (vane) width
n'_{struts}		Number of struts
σ'_{shroud}		Stress on shroud
ρ'	kg/mm^3	Density
c'	\$/mm^3	Cost density
Performance parameters		
W	kg	Weight of the strut
c_{raw}	\$	Raw material cost
c_s	\$	Cost of the shroud
W_s	kg	Weight of the shroud
Target thresholds		
Node Symbol	**Units**	**Description**
e_1 F_{axial}	N	Compressive force on strut
e_2 σ_{max}	MPa	Maximum stress on strut
e_3 $n^{threshold}_{struts}$	MPa	Required number of struts
e_4 B	N	Bearing load on shroud
Decided values		
e_1 $F_{buckling}$	N	Buckling load of strut
e_2 σ_y	MPa	Yield stress
e_3 n_{struts}	MPa	Number of struts
e_4 B_{max}	N	Maximum supported load

4.5 Step 6: Construction of the margin value plot

Figure 5 shows the MVPs corresponding to each alternative in Table 2 and a neutral line represented by a dotted line that passes through points (I_{min}, A_{min}) and (I_{max}, A_{max}).

Accepted Manuscript Not Copyedited

Downloaded from http://asmedigitalcollection.asme.org/mechanicaldesign/article-pdf/doi/10.1115/1.4063966/7056417/md-23-1056.pdf by McGill University user on 06 November 2023

Journal of Mechanical Design, ASME, October 2023;
Accepted manuscript posted October 21, 2023. doi:10.1115/1.4063966
Copyright © 2023 by ASME

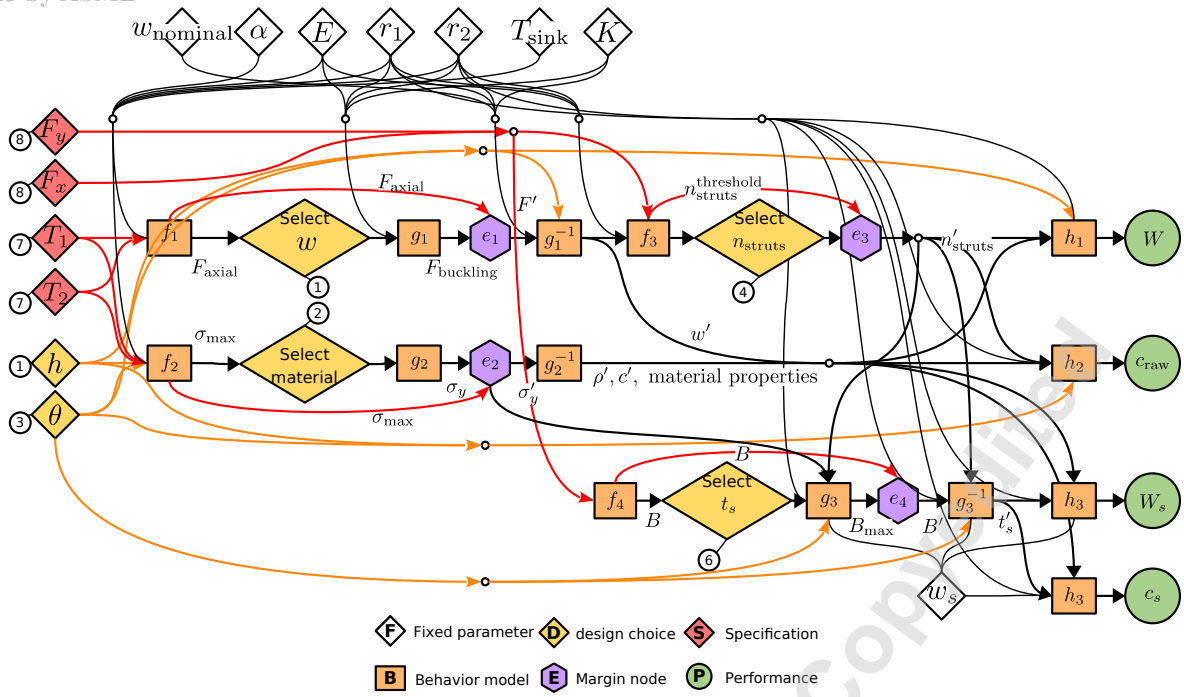

Fig. 4: MAN for performing margin analysis on concepts with circumferential shrouds.

The x and y axes are normalized by the maximum and minimum impact and absorption, respectively, such that they are confined to the range (0,1). This places equal weighting on the margins' IoP and CAC values.

Recall in Step 5 that 1000 samples were drawn for each conceptual alternative in Table 2. For each of these samples, the IoP and CAC are each averaged over the performance parameters and input specifications, respectively. Recall that impact is a matrix $\mathbf{I} \in \mathbb{R}^{n \times n_{\text{perfs}}}$, the average impact of margin node e_i is obtained by averaging the elements of the ith row of $\mathbf{I}$ to obtain I_i. A similar process is used for the average absorption A_i.

The results of averaging CAC and IoP considering the variation in input specification values for each margin node (represented by the color code) in the context of each concept (represented by the shapes of the points) are shown in Figure 5. The figure also shows the distance $v_{\text{design},i}$ for each margin node as obtained by Equation (1) which represents the value of each margin node. Margin nodes below the neutral line have a negative value, while those above have a positive value. The total value of each concept is calculated by summing the individual values of each margin node.

$$v_{\text{design}} = \sum_{i=1}^{n} v_{\text{design},i}. \tag{2}$$

Equation (2) implies equal weighting for the value of each margin node. Weighted averages can be used in lieu of Equation (2) to place more emphasis on certain margin nodes. Table 4 shows the computed value for each margin node and conceptual alternative, as well as their reliability

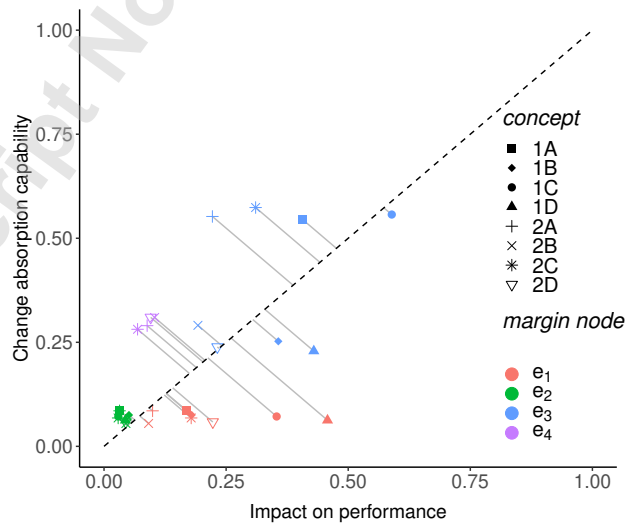

Fig. 5: MVP plot of average IoP, CAC, and distance to the neutral line for eight different conceptual designs (denoted by shape) and their corresponding nodes (denoted by color). See Table 4 for details of the concepts.

given by the ratio of the number of supported input specifications to the total number of samples.

In this case, the preferred concept is **2A** because it has the greatest value for its margin nodes. However, it has low reliability (677 of 1000). This implies that value does not always translate to reliability and a more conservative choice could be concept **1A** if more than 90% reliability is desired.

Having explained the methodology for the simple case of eight alternatives, we move on to explain how it can be applied to analyze the large numbers of concepts arising

Accepted Manuscript Not Copyedited

Downloaded from http://asmedigitalcollection.asme.org/mechanicaldesign/article-pdf/doi/10.1115/1.4063966/7056417/md-23-1056.pdf by McGill University user on 06 November 2023

Journal of Mechanical Design. Received February 01, 2023;
Accepted manuscript posted October 21, 2023. doi:10.1115/1.4063966
Copyright © 2023 by ASME

Table 4: Value of concepts in the limited example.

Concept	MAN	Choices h (mm)	Choices θ (°)	Value v_{design}	Reliability $P(\mathbf{e} \geq \mathbf{0})$
1A	Fig. S.III	15	0	0.0737	0.932
1B		15	30	-0.1260	1.000
1C		17	0	-0.1850	0.907
1D		17	30	-0.3930	1.000
2A	Fig. 4	15	0	0.3890	0.677
2B		15	30	0.1900	0.883
2C		17	0	0.2760	0.551
2D		17	30	0.0482	0.842

from all possible conceptual alternatives that can be enumerated from Table 1. The results of this analysis are shown using the parallel coordinates plot (PCP) in Figure 6 to visualize multi-dimensional data [53]. The PCP was generated using an open-source online tool [54].

In the next section, we examine the MVPs and PCP in greater detail to show how it is possible to obtain design insight from this method.

5 Results and discussion

5.1 Analysis of the limited example

To recap, Figure 5 provides a visual representation of the different margin nodes in the system by aggregating the IoP and CAC across performance parameters and input specifications, respectively and then averaging IoP and CAC over the input specification samples. The first aggregation operation obscures the correlation between IoP and CAC. The IoP and CAC matrices reveal these correlations and provide insight into the dependencies in the MAN to gauge the trade-off between each CAC and IoP at each margin node. We examine this correlation by performing a pairwise comparison between the elements of the IoP and CAC matrices of concept **1A** from the limited example in Figure 7. We observe that margin nodes e_1 and e_3 are positively correlated in terms of impact on weight W and raw material cost c_{raw}. Increasing excess margin in nodes e_1 or e_3 will result in an increase in the impact on weight W and cost c_{raw}. Conversely, an increase in excess margin node e_2 results in an increase in the impact on weight W and a decrease in the impact on raw material cost c_{raw} with a Pearson correlation coefficient of -0.890. This is because margin node e_2 pertains to the excess margin resulting from the material selection. In our model, the materials considered were steel, Inconel, and titanium arranged in order of increasing unit cost and decreasing material density. Titanium alloys are the least dense but cost more than the denser steel alloys.

There is a large positive correlation between the absorption of T_1 and the absorption of T_2 (Pearson correlation coefficients of 1.00, 1.00, and 0.995 for margin nodes e_1, e_2, and e_3) because all target thresholds are functions of the temperature gradient $T_1 - T_2$ resulting in identical change absorption mechanisms. Finally, there is no correlation between change absorption against the bearing loads B_x and B_y and any other IoP or CAC for margin nodes e_1 and e_2. This is because the bearing loads do not interact in any way with margin nodes e_1 and e_2. The previous analyses serve as examples showing how the designer can gain a deeper understanding of the dependencies in the MAN.

There is little to no positive correlation between the CAC against the temperature loads T_1 and T_2 and the IoP of weight W and cost c_{raw} for margin nodes e_1 and e_2. The positive correlation is stronger for margin node e_3 since any attempt to absorb change in the temperature loads through margin node e_3 will result in a large weight and cost increase due to the addition of new struts. This implies that the trade-off between CAC against T_1 and T_2 and impact on cost c_{raw} and weight W is more pronounced at margin node e_3 and the designer should prioritize margin nodes e_1 and e_2 for absorbing temperature changes. This example shows how the designer can gauge the trade-offs throughout the design by examining correlations in CAC and IoP.

Further, averaging across input specification samples shown in Figure 5 discards the distribution of the calculated CAC and IoP. This information can be used to assess the risk that a change will propagate or the performance of the design will be impacted. We examine the samples for concept **1A** of the limited example before aggregation and their frequency distributions in Figure 8a. Examination of this figure reveals high-density regions of the MVP, which are populated by different design decisions.

The points for margin node e_3 and their corresponding marginal cumulative frequency distributions are color-coded on the MVP in Figure 8b. This allows designers to discern the probability of change propagation from one decision to the next as reported by Brahma et al. [50]. For example, the probability of revising decision 3 (shown in green) due to the need for higher CAC (beyond 3.03) is less than 0.15 ($1 - 0.859$ labeled in the right inset of the figure). This will result in an IoP less than 0.132 (top inset of the figure). This analysis helps designers gauge the robustness of an existing design to change in input specifications. Decision 3 with 12 Inconel 70 mm thick struts provides good robustness against the input specifications as it accounts for most of the decisions taken (see Figure S.V in the supplemental material). This decision can serve as a starting point for a more refined DSE or for negotiating the input specifications so that they fall within the capability of decision 3. We will now examine the extended example involving 13,104 conceptual alternatives.

5.2 Analysis of the extended example

We sampled 100 input specifications for each conceptual alternative from the PDFs in Table 1. This allowed calculation of each margin node's expected IoP and CAC. Reliability was calculated similarly to the limited example in Section 4.5. Of the 13,104 conceptual alternatives, only 3,355 feasible alternatives remained with reliability > 0. Figure 6 shows the value of the feasible conceptual alternatives. The color scale shows the value v_{design} of each alternative, with orange being the highest. It can be observed that the most valuable conceptual alternatives are not nec-

Accepted Manuscript Not Copyedited

Downloaded from http://asmedigitalcollection.asme.org/mechanicaldesign/article-pdf/doi/10.1115/1.4063966/7056417/md-23-1056.pdf by McGill University user on 06 November 2023

Journal of Mechanical Design. Received February 01, 2023;
Accepted manuscript posted October 21, 2023. doi:10.1115/1.4063966
Copyright © 2023 by ASME

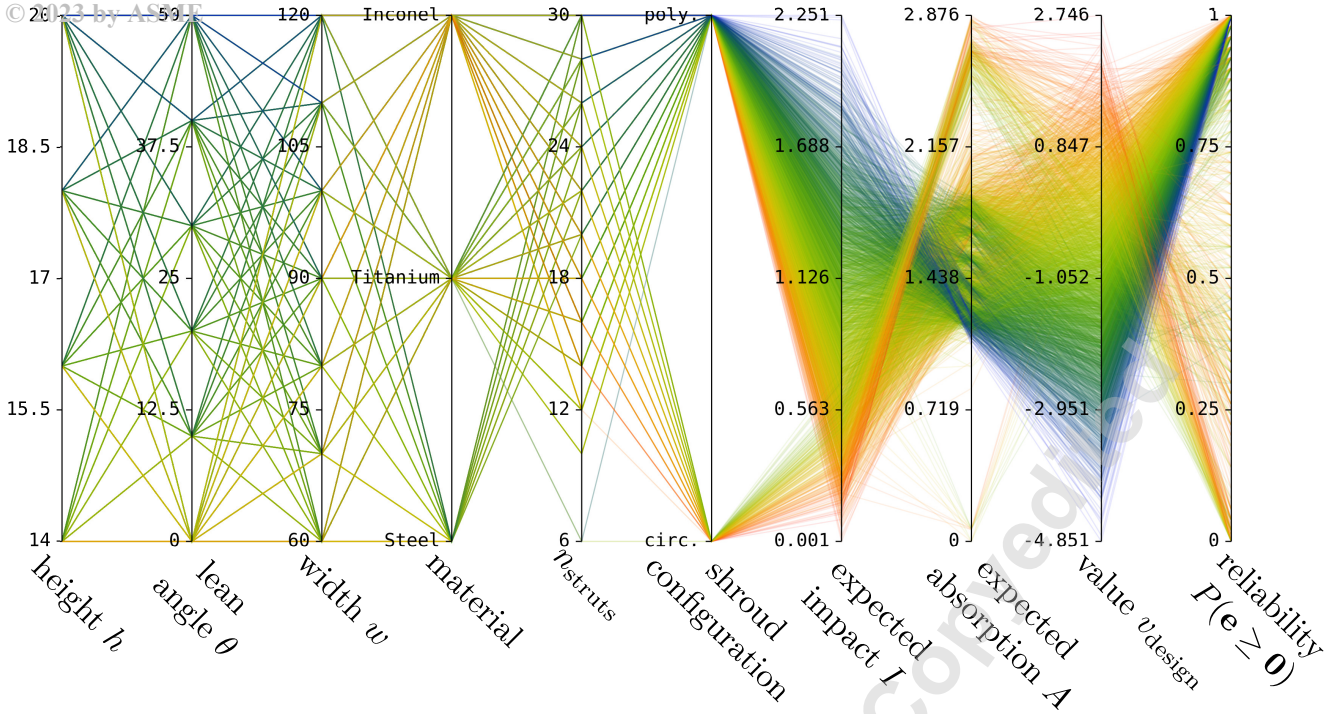

Fig. 6: Parallel coordinates plot showing the results of evaluating all possible conceptual alternatives for the extended example using the MVM. Of the 13,104 concepts only 3,356 feasible concepts are shown. The color scale represents the value metric v_{total} for each feasible concept (with orange being the highest and blue being the lowest).

essarily the most reliable, which is in line with observations from the limited example (concept **1A** versus concept **2A**). The designer may want to select conservative alternatives that still offer high value in terms of margins.

We now investigate the effect of the margin allocation strategy on the value of the conceptual alternatives. To recap, a minimum excess allocation strategy was used to develop the analysis discussed thus far (See Section 4.4). To do this, the calculations for the 6,552 conceptual alternatives with polygonal shrouds were run for a deterministic set of input specifications $T_1 = 434\ ^{o}C$, $T_2 = 432\ ^{o}C$, $B_x = 80\ N$, $B_y = 80\ N$ to eliminate the effect of uncertainty in input specifications on the design's value. Of the 6,552 conceptual alternatives, only 3,165 feasible alternatives remained (with excess $\mathbf{e} \geq \mathbf{0}$).

The feasible alternatives are evaluated and displayed in Figure 9 (shown in grey). We compare them to a case where the design choices associated with margin nodes (i.e., width, material choices, and number of struts) are allocated according to the minimum excess strategy, while the width h and lean angle θ are varied according to a full factorial design as part of DSE. This results in an additional 24 alternatives (4 and 6 choices for h and θ, respectively), of which only 5 are feasible (shown in blue). We can see that a slightly better margin allocation strategy is discovered by enumerating and evaluating all the design choices $v_{\text{design}} = 1.5708$ (shown in red) as opposed to a minimum excess strategy which results in a maximum $v_{\text{design}} = 1.4104$ (shown in blue). This implies that different strategies could be explored in future work to identify the most valuable conceptual alternatives. However, for this particular example, the minimum excess strategy performs well relative to the most valuable conceptual alternative discovered by enumeration of all the concepts. Table 5 shows the top-performing design choices and corresponding value metrics for both margin allocation strategies. It can be seen that the minimum excess strategy resulted in a design with higher overall weight relative to the best-known design from a full factorial design. This is because Inconel (which has higher material density) resulted in less excess margin e_2 compared to e_3. Therefore, exploring the design space before committing to a solution obtained by minimum excess is important.

5.3 Discussion

The new framework addresses several gaps found in the literature. Firstly, it addresses both parametric and incremental design domains, as demonstrated in the examples. The use of Brahma and Wynn's MVM enables margins which inadvertently get included in a design to be utilized as uncertainty absorbers [12]. A limitation of existing approaches, mentioned earlier, is that they generally do not relate product information with the physical design. The approaches that do consider it do not suggest methods to rank the solutions generated. We address this limitation by incorporating the functional perspective to generate and explore the design space. By using the EF-M approach, the product information is related to the physical design. Further, only a few contributions consider margins in the context of DSE (e.g., [40, 45]). However, such papers do not consider both the desirable and undesirable effects of margins, as represented by IoP and CAC in this paper. We

Accepted Manuscript Not Copyedited

Downloaded from http://asmedigitalcollection.asme.org/mechanicaldesign/article-pdf/doi/10.1115/1.4063966/7056417/md-23-1056.pdf by McGill University user on 06 November 2023

Journal of Mechanical Design. Received February 01, 2023;
Accepted manuscript posted October 21, 2023. doi:10.1115/1.4063966
Copyright © 2023 by ASME

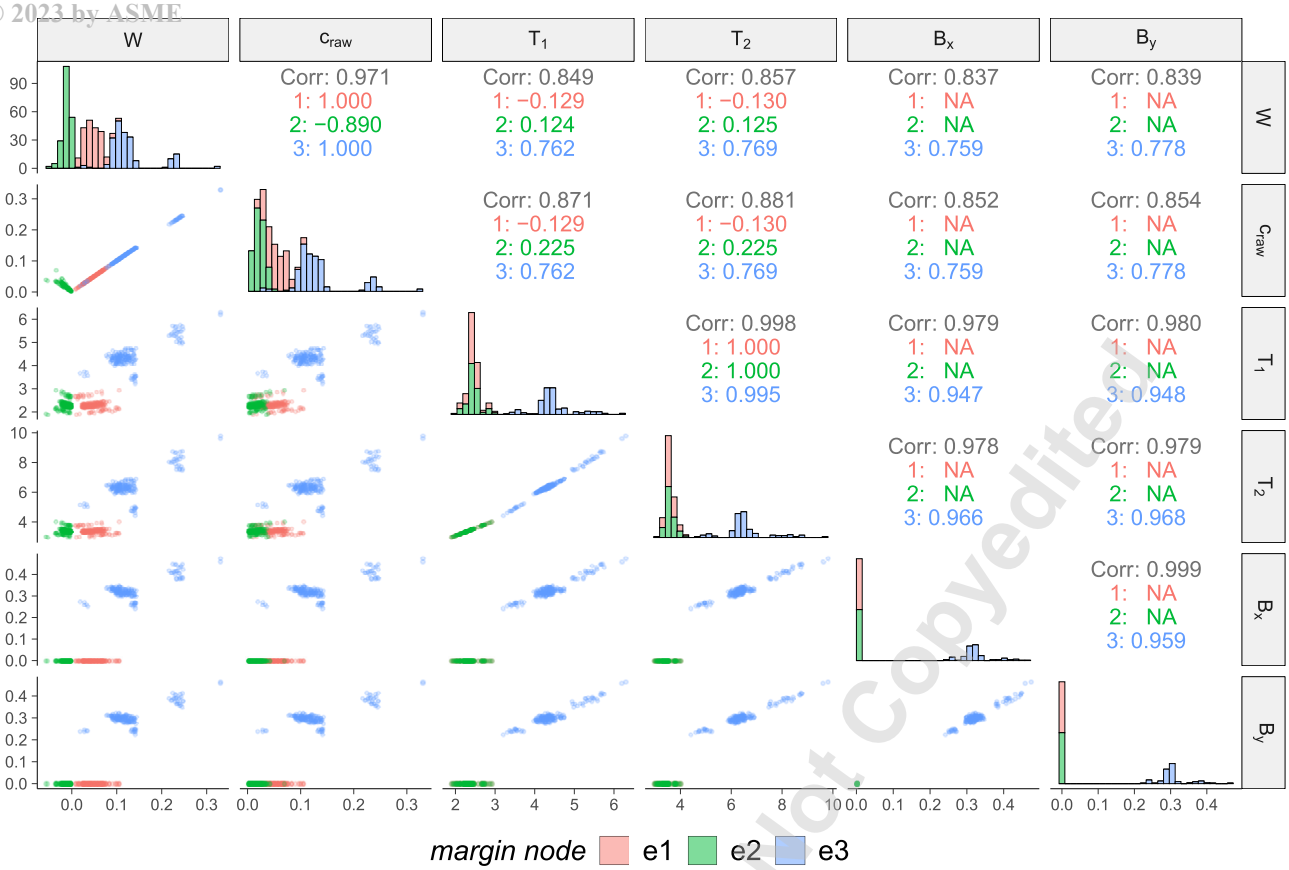

Fig. 7: Scatter plot matrix of IoP and CAC of conceptual alternative **1A** ($\theta = 0^o$, and $h = 15$ mm, polygonal shroud) . Elements of the IoP and CAC matrices are represented by their corresponding performance parameters and input specifications, respectively. The diagonal plots represent the marginal distribution of each matrix element, while the off-diagonal plots represent the correlation plots between the marginal distributions for each matrix element. The variation arises from the variation in input specifications.

Table 5: Best performing conceptual alternatives in Figure 9.

Strategy	choices **d**					**Relative excess**			**Performance**		**Value metrics**		
	h (mm)	θ (^{o})	w (mm)	material	n_{struts}	e_1	e_1	e_3	weight (kg)	cost ($)	IoP	CAC	v_{design}
min. excess	14	0	90	Inconel	8	0.0294	0.0176	0.2810	15.69	9.41	0.1032	2.4642	1.4104
DOE	14	0	90	Titanium	8	0.0294	0.8318	0.3333	8.48	9.33	0.0435	2.4642	1.5708

argue that for an effective ranking of the generated designs, both IoP and CAC must be considered and neglecting them may result in misleading or overdesigned solutions that impact performance with little margin to absorb change propagation and other uncertainties. Another limitation of existing methods is the lack of explicit approaches, e.g., in ref. [10], to identify the set of feasible solutions from the set of a large number of combinatorially generated concepts. The approach presented in this paper addresses this by defining the feasibility of a solution in terms of excess margin. Since negative excess is impracticable, feasibility is decided by identifying solutions which have margin $>= 0$. For the example case, this is presented in Section 5.2.

Further, we investigated multiple approaches for allocating margins during DSE. There are advantages and disadvantages of the minimum excess and DOE-based strategies that are compared in Figure 9. An advantage of the minimum excess strategy is that it involves varying far fewer independent design variables (in this case h and θ) as opposed to the DOE-based strategy, which in this case involved 5 variables. The reduction in the number of independent variables results in reduced computational cost (in this case, 6,552 vs 24 evaluations for the DOE-based and minimum excess strategies, respectively). The disadvantage of the minimum excess strategy in comparison to the DOE-based strategy is the potential to overlook good alternatives due to the constraints placed on the decision variables. Future work could focus on numerical optimization strategies for exploring multi-dimensional spaces efficiently without having to evaluate a large number of alternatives.

The presented approach also has some limitations associated with the current implementation of the MVM. The MVM relies on iteration to find the deterioration in input specifications necessary for computing CAC resulting in poor scaling with a large number of input specifications.

Accepted Manuscript Not Copyedited

Downloaded from http://asmedigitalcollection.asme.org/mechanicaldesign/article-pdf/doi/10.1115/1.4063966/7056417/md-23-1056.pdf by McGill University user on 06 November 2023

Journal of Mechanical Design. Received February 01, 2023;
Accepted manuscript posted October 21, 2023. doi:10.1115/1.4063966
Copyright © 2023 by ASME

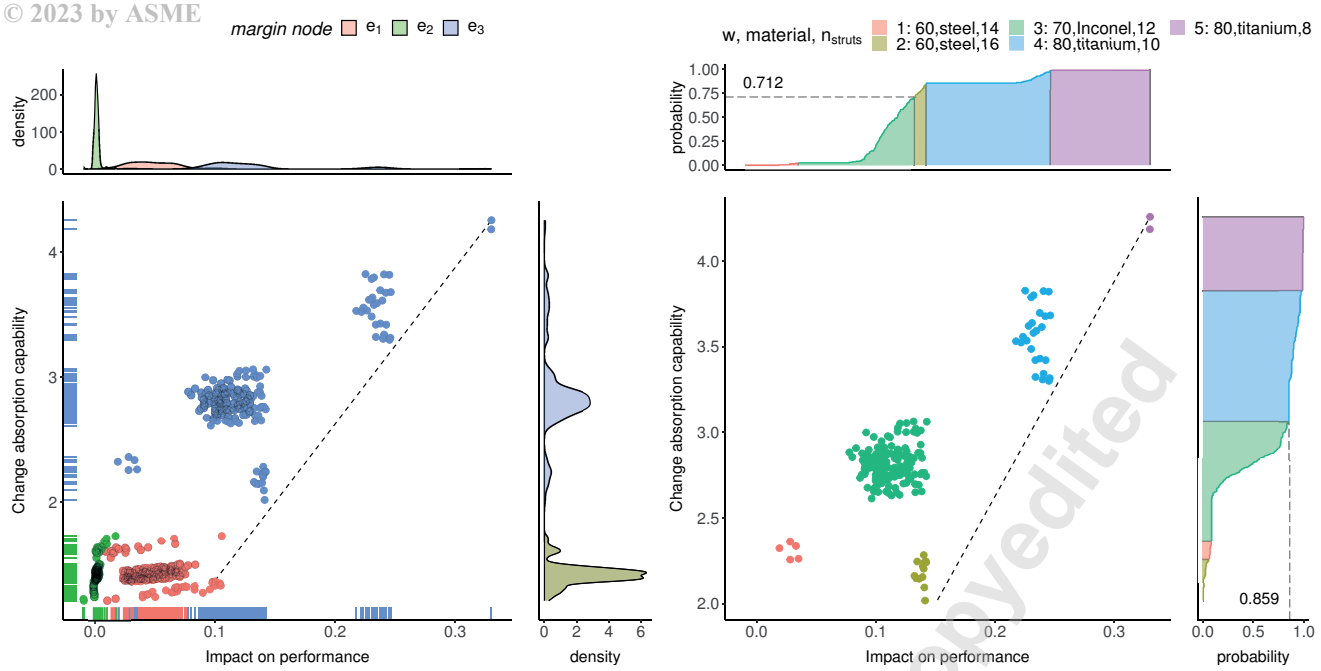

(a) (b)

Fig. 8: MVP of the concept when $\theta = 0^{o}$, and $h = 15$ mm. (a) shows the marginal frequency distribution (note that the marginal distribution of CAC for e_1 is identical to e_2) and (b) shows the marginal cumulative frequency distribution of margin node e_3. The clusters are color-coded to represent the design decisions.

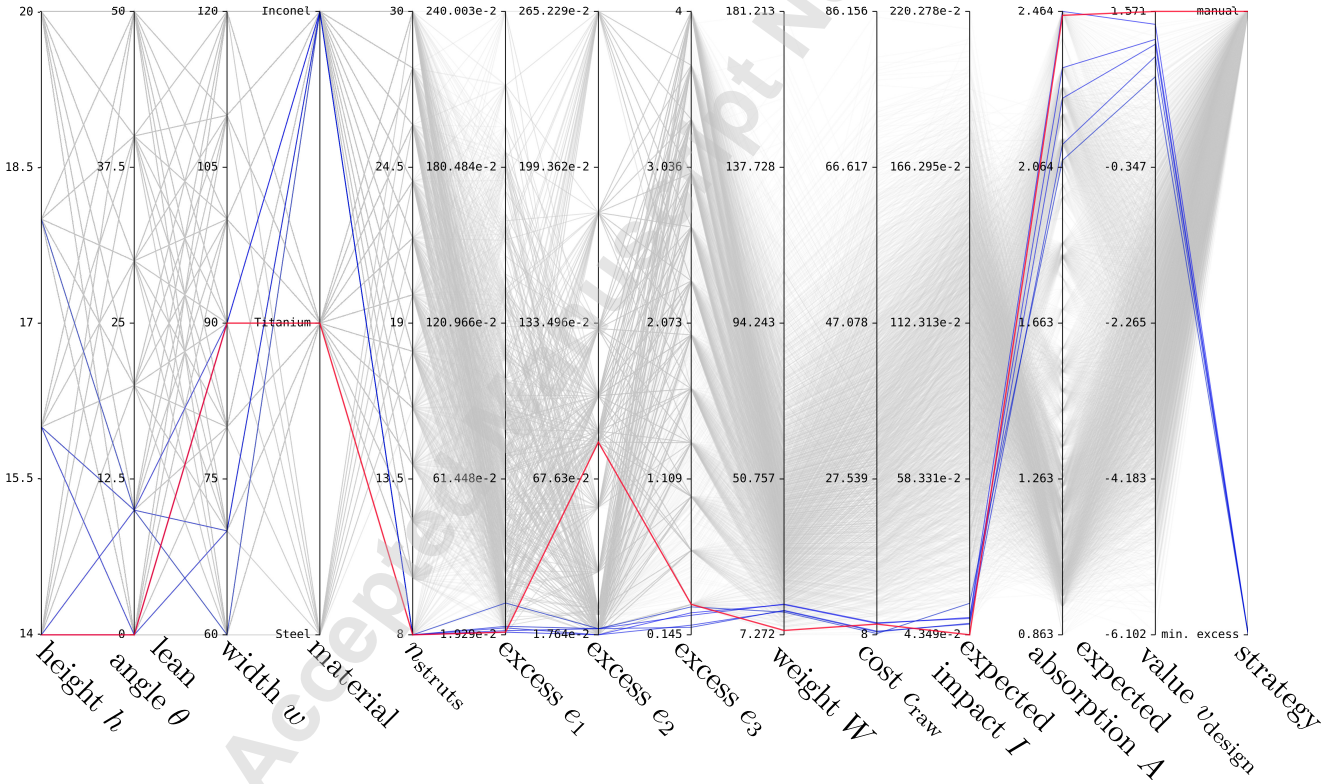

Fig. 9: Parallel coordinates plot showing the results of evaluating all possible conceptual alternatives using a deterministic set of input specifications $\mathbf{s} = [434\ ^{o}\text{C}, 432\ ^{o}\text{C}, 80\ \text{N}, 80\ \text{N}]^{\mathsf{T}}$. Blue lines represent concepts obtained by using the minimum excess strategy for margin allocation. The red line shows the best-performing alternative.

Future approaches could use surrogate modeling and classification approaches to identify a surface that describes the maximum deterioration in the space of the input specifications. Finally, the results shown are valid only for the ex-

Accepted Manuscript Not Copyedited

Downloaded from http://asmedigitalcollection.asme.org/mechanicaldesign/article-pdf/doi/10.1115/1.4063966/7056417/md-23-1056.pdf by McGill University user on 06 November 2023

Journal of Mechanical Design. Received February 01, 2023;
Accepted manuscript posted October 21, 2023. doi:10.1115/1.4063966
Copyright © 2023 by ASME

amples in this paper, so the approach should be tested on additional cases that involve concept generation and evaluation. The presented approach is flexible enough to encompass a wide range of practical design problems, where the designers are free to specify their own performance parameters, margins, decisions, input specifications, and the models that govern them.

6 Conclusion

It is desirable to consider a wide range of concepts early in the design process, selecting those that offer high performance as well as the ability to absorb later design changes. This paper has addressed the task with a new design space exploration (DSE) framework that helps to bridge the gap between abstract conceptual models and preliminary analysis models during the early stages of design. The framework utilizes a functional model based on enhanced function-means trees to enumerate conceptual alternatives, which are then evaluated using the margin value method. The enumerated concepts are narrowed down to feasible concepts that satisfy the requirements and are further distilled by evaluating their value in terms of design margins. In particular, Margin value plots are used to gauge the trade-off between the concepts' impact on performance and change absorption capability by examining how they are correlated. The framework also allows estimation of the probability of change propagation involving concepts by examining reliability under variation in input specifications. Insights regarding the most valuable and reliable designs obtained from the framework allow designers to use said designs for a refined DSE or for negotiating the input specification ranges during product development. In conclusion, the presented framework shows how it is possible to generate and select suitable high-performing concepts given the uncertainties in early design phases.

Acknowledgements

The authors of this paper acknowledge financial support from the Area of Advance at Chalmers University, and the partial financial support of their work through NSERC discovery grant 436193-2018.

Data availability statement

The MVM in this manuscript is implemented as an open source library, `mvmlib` [55]. The visualizations and examples in this paper are available on a code repository [56].

References

[1] J. K. Allen, C. Seepersad, H. Choi, and F. Mistree. Robust design for multiscale and multidisciplinary applications. *ASME J Mech Des*, 128(4):832–843, 01 2006. doi: 10.1115/1.2202880.

[2] D. C. Wynn and P. J. Clarkson. Process models in design and development. *Res Eng Des*, 29(2):161–202, jul 2018. doi: 10.1007/s00163-017-0262-7. URL https://link.springer.com/article/10.1007/s00163-017-0262-7.

[3] B. M. Kennedy, D. K. Sobek, and M. N. Kennedy. Reducing rework by applying set-based practices early in the systems engineering process. *Syst Eng*, 17(3):278–296, 2014. doi: 10.1002/sys.21269.

[4] D. K. Sobek II, A. C. Ward, and J. K. Liker. Toyota's principles of set-based concurrent engineering. *MIT Sloan Management Review*, 40(2):67, 1999.

[5] S. Krish. A practical generative design method. *Comput Aided Des*, 43(1):88–100, 2011. doi: 10.1016/j.cad.2010.09.009. URL https://doi.org/10.1016/j.cad.2010.09.009.

[6] F. Buonamici, M. Carfagni, R. Furferi, Y. Volpe, and L. Governi. Generative design: an explorative study. *Comput Aided Des Appl*, 18(1), 2021. doi: 10.14733/cadaps.2021.144-155.

[7] A. Panesar, M. Abdi, D. Hickman, and I. Ashcroft. Strategies for functionally graded lattice structures derived using topology optimisation for additive manufacturing. *Addit Manuf*, 19:81–94, 2018. doi: 10.1016/j.addma.2017.11.008. URL https://www.sciencedirect.com/science/article/pii/S221486041730115X.

[8] D. Vlah, R. Žavbi, and N. Vukašinović. Evaluation of topology optimization and generative design tools as support for conceptual design. *Proceedings of the Design Society: DESIGN Conference*, 1:451–460, 2020. doi: 10.1017/dsd.2020.165.

[9] R. F. Woodbury and A. L. Burrow. Whither design space? *Ai Edam*, 20(2):63–82, 2006. doi: 10.1017/S0890060406060057. URL https://doi.org/10.1017/S0890060406060057.

[10] J. R. Müller, O. Isaksson, J. Landahl, V. Raja, M. Panarotto, C. Levandowski, and D. Raudberget. Enhanced function-means modeling supporting design space exploration. *AIEDAM*, 33(4):502–516, 2019. doi: 10.1017/S0890060419000271. URL https://doi.org/10.1017/S0890060419000271.

[11] J. R. Müller, M. Panarotto, and O. Isaksson. Function model-based generation of CAD model variants. *Comput Aided Des Appl*, 18(5):970–989, 2021. doi: 10.14733/cadaps.2021.970-989. URL https://doi.org/10.14733/cadaps.2021.970-989.

[12] A. Brahma and D. C. Wynn. Margin value method for engineering design improvement. *Res Eng Des*, 31(3):353–381, 2020. doi: 10.1007/s00163-020-00335-8. URL https://doi.org/10.1007/s00163-020-00335-8.

[13] E. Kang, E. Jackson, and W. Schulte. An approach for effective design space exploration. In Radu Calinescu and Ethan Jackson, editors, *Foundations of Computer Software. Modeling, Development, and Verification of Adaptive Systems*, pages 33–54, Berlin, Heidelberg, 2011. Springer Berlin Heidelberg. doi: 10.1007/978-3-642-21292-5_3. URL https://doi.org/10.1007/978-3-642-21292-5_3.

[14] R. Wang, A. B. Nellippallil, G. Wang, Y. Yan, J. K. Allen, and F. Mistree. Systematic design space exploration using a template-based ontological method. *Adv Eng Inform*, 36:163–177, 2018. doi: 10.1016/j.aei.2018.03.006. URL https://doi.org/10.1016/j.aei.2018.03.006.

[15] M. Turrin, P. Von Buelow, and R. Stouffs. Design explorations of performance driven geometry in architectural design using parametric modeling and genetic algorithms. *Adv Eng Inform*, 25(4):656–675, 2011. doi: 10.1016/j.aei.2011.07.009. URL https://doi.org/10.1016/j.aei.2011.07.009.

[16] A. Duffy, M. M. Andreasen, K. J. MacCallum, and L. N. Reijers. Design coordination for concurrent engineering. *J Eng Des*, 4(4):251–265, 1993. doi: 10.1080/09544829308914785.

[17] J. E Folkestad and R. L. Johnson. Resolving the conflict between design and manufacturing: integrated rapid prototyping and rapid tooling (irprt). *J Ind Technol*, 17(4):1–7, 2001.

[18] K. B. Clark and T. Fujimoto. *Product Development Performance: Strategy, Organization, and Management in the World Auto Industry*. Harvard Business School Press, 1991. ISBN 9780875842455.

[19] A. C. Ward, J. K. Liker, D. K. Sobek, and J. J. Cristiano. Set-based concurrent engineering and toyota. In *International Design Engineering Technical Conferences and Computers and Information in Engineering Conference*, volume 12822, pages 79–90. ASME, 1994. doi: 10.1115/DETC1994-0009.

[20] H. Mokhtarian, E. Coatanéa, and H. Paris. Function modeling combined with physics-based reasoning for assessing design options and supporting innovative ideation. *AIEDAM*, 31(4):476–500, nov 2017. doi: 10.1017/S0890060417000403. URL https://doi.org/10.1017/S0890060417000403.

[21] J. S. Gero and U. Kannengiesser. The situated function–behaviour–structure framework. *Des Stud*, 25(4):373–391, 2004. doi: 10.1016/j.destud.2003.10.010. URL https://doi.org/10.1016/j.destud.2003.10.010.

[22] E. C. e Costa, J. Jorge, A. D. Knochel, and J. P. Duarte. Enabling parametric design space exploration by non-designers. *AI EDAM*, 34(2):160–175, 2020. doi: 10.1017/S0890060420000177. URL https://doi.org/10.1017/S0890060420000177.

[23] P. N. Koch, J. P. Evans, and D. Powell. Interdigitation for effective design space exploration using isight. *Struct Multidiscipl Optim*, 23(2):111–126, 2002. doi: 10.1007/s00158-002-0171-9. URL https://doi.org/10.1007/s00158-002-0171-9.

[24] N. Ahmad, D. C. Wynn, and P. J. Clarkson. Change impact on a product and its redesign process: a tool for knowledge capture and reuse. *Res Eng Des*, 24(3):219–244, 2013. doi: 10.1007/s00163-012-0139-8. URL https://doi.org/10.1007/s00163-012-0139-8.

[25] D. Raudberget. Practical applications of set-based concurrent engineering in industry. *Journal of Mechanical Engineering*, 56(11):685–695, 2010.

[26] D. M. Upton. The management of manufacturing flexibility. *California Man-*

Downloaded from http://asmedigitalcollection.asme.org/mechanicaldesign/article-pdf/doi/10.1115/1.4063966/7056417/md-23-1056.pdf by McGill University user on 06 November 2023

Accepted Manuscript Not Copyedited

Journal of Mechanical Design. Received February 01, 2023;
Accepted manuscript posted October 21, 2023. doi:10.1115/1.4063966
Copyright © 2023 by ASME

agement Review, 36(2):72–89, 1994. doi: 10.2307/41165745.

[27] S. Lebjioui. *Investigating and managing design margins throughout the product development process*. PhD thesis, Open University (United Kingdom), 2018.

[28] Hugh L McManus, Daniel E Hastings, and Joyce M Warmkessel. New methods for rapid architecture selection and conceptual design. *Journal of Spacecraft and Rockets*, 41(1):10–19, 2004.

[29] Joseph H Saleh, Gregory Mark, and Nicole C Jordan. Flexibility: a multidisciplinary literature review and a research agenda for designing flexible engineering systems. *Journal of Engineering Design*, 20(3):307–323, 2009.

[30] Genichi Taguchi and Don Clausing. Robust quality. *Harvard Business Review*, 68(1):65 – 75, 1990. ISSN 00178012.

[31] Prithviraj Banerjee and Olivier L de Weck. Flexibility strategy-valuing flexible product options. In *ICSE Conference on Synergy Between Systems Engineering and Project Management. Las Vegas, NV, INCOSE*. Citeseer, 2004.

[32] Gyung-Jin Park, Tae-Hee Lee, Kwon Hee Lee, and Kwang-Hyeon Hwang. Robust design: an overview. *AIAA journal*, 44(1):181–191, 2006.

[33] Wei Chen, J. K. Allen, Kwok-Leung Tsui, and F. Mistree. A Procedure for Robust Design: Minimizing Variations Caused by Noise Factors and Control Factors. *Journal of Mechanical Design*, 118(4):478–485, 12 1996. doi: 10.1115/1.2826915.

[34] Serghei Floricel and Roger Miller. Strategizing for anticipated risks and turbulence in large-scale engineering projects. *International Journal of project management*, 19(8):445–455, 2001.

[35] Tzyy-Shuh Chang, Allen C Ward, Jinkoo Lee, and Edwin H Jacox. Conceptual robustness in simultaneous engineering: an extension of taguchi's parameter design. *Research in Engineering Design*, 6:211–222, 1994.

[36] Arindam Brahma, Scott Ferguson, Claudia Eckert, and Ola Isaksson. Margins in design – review of related concepts and methods. *Journal of Engineering Design*, 0(0):1–34, 2023. doi: 10.1080/09544828.2023.2225842.

[37] Lorenzo P Pagani. *On the quantification of safety margins*. PhD thesis, Massachusetts Institute of Technology, 2004.

[38] C. Eckert, O. Isaksson, S. Lebjioui, C. F. Earl, and S. Edlund. Design margins in industrial practice. *Des Sci*, 6, 2020. doi: 10.1017/dsj.2020.19.

[39] A. Brahma and D. C. Wynn. A study on the mechanisms of change propagation in mechanical design. *ASME J Mech Des*, 143(12), 2021. doi: 10.1115/1.4050927. URL https://doi.org/10.1115/1.4050927.

[40] M. D. Guenov, X. Chen, A. Molina-Cristóbal, A. Riaz, A. van Heerden, and M. Padulo. Margin allocation and tradeoff in complex systems design and optimization. *AIAA J*, 56(7):2887–2902, 2018. doi: 10.2514/1.J056357. URL https://doi.org/10.2514/1.J056357.

[41] C. Eckert, O. Isaksson, and C. Earl. Design margins: a hidden issue in industry. *Des Sci*, 5:e9, may 2019. doi: 10.1017/dsj.2019.7. URL https://www.cambridge.org/core/product/identifier/S2053470119000076/type/journal_article.

[42] G. A Fenton, F. Naghibi, D. Dundas, R. J. Bathurst, and D. V. Griffiths. Reliability-based geotechnical design in 2014 canadian highway bridge design code. *Can Geotech J*, 53(2):236–251, 2015. doi: 10.1139/cgj-2015-0158. URL 10.1139/cgj-2015-0158.

[43] E. A. Mohammed, S. D. Benson, S. E. Hirdaris, and R. S. Dow. Design safety margin of a 10,000 teu container ship through ultimate hull girder load combination analysis. *Mar Struct*, 46:78–101, 2016. doi: 10.1016/j.marstruc.2015.12.003. URL 10.1016/j.marstruc.2015.12.003.

[44] A. H. Tilstra, P. B. Backlund, C. C. Seepersad, and K. L. Wood. Principles for designing products with flexibility for future evolution. *I J Mass C*, 5(1):22–54, 2015. doi: 10.1115/DETC2007-35695. URL http://dx.doi.org/10.1115/DETC2007-35695.

[45] J. Tan, K. Otto, and K. Wood. Concept design trade-offs considering performance margins. *DS 85-1: Proceedings of NordDesign 2016, Volume 1, Trondheim, Norway, 10th-12th August 2016*, pages 421–429, 2016.

[46] E. Z Cansler, S. B. White, S. M. Ferguson, and C. A. Mattson. Excess identification and mapping in engineered systems. *ASME J Mech Des*, 138(8), 2016. doi: 10.1115/1.40338845. URL https://doi.org/10.1115/1.40338845.

[47] P. J. Clarkson, C. Simons, and C. Eckert. Predicting change propagation in complex design. *J. Mech. Des.*, 126(5):788–797, 2004. doi: 10.1115/1.1765117. URL http://dx.doi.org/10.1115/1.1765117.

[48] K. Al Handawi, M. Panarotto, P. Andersson, O. Isaksson, and M. Kokkolaras. Optimization of Design Margins Allocation When Making Use of Additive Remanufacturing. *ASME J Mech Des*, 144:1–18, 2021. doi: 10.1115/1.4051607. URL http://asmedigitalcollection.asme.org/mechanicaldesign/article-pdf/144/1/012001/6730339/md_144_1_012001.pdf.

[49] M. A. Bouhlel, J. T. Hwang, N. Bartoli, R. Lafage, J. Morlier, and J. R. R. A. Martins. A python surrogate modeling framework with derivatives. *Adv Eng Softw*, page 102662, 2019. doi: 10.1016/j.advengsoft.2019.03.005. URL https://doi.org/10.1016/j.advengsoft.2019.03.005.

[50] A. Brahma, D. C. Wynn, and O. Isaksson. Use of margin to absorb variation in design specifications: An analysis using the margin value method. *Proceedings of the Design Society*, 2:323–332, 2022. doi: 10.1017/pds.2022.34.

[51] M. J. Chalupnik, D. C. Wynn, and P. J. Clarkson. Comparison of ilities for protection against uncertainty in system design. *J Eng Des*, 24:814–829, 12 2013. doi: 10.1080/09544828.2013.851783. URL http://www.tandfonline.com/doi/abs/10.1080/09544828.2013.851783.

[52] V. Raja, M. Kokkolaras, and O. Isaksson. A simulation-assisted complexity metric for design optimization of integrated architecture aero-engine structures. *Struct Multidiscipl Optim*, 60(1):287–300, 2019. doi: 10.1007/s00158-019-02308-5. URL https://link.springer.com/article/10.1007/s00158-019-02308-5.

[53] A. Inselberg. The plane with parallel coordinates. *Vis Comput*, 1(4):69–91, dec 1985. doi: 10.1007/BF01898350. URL https://link.springer.com/article/10.1007/BF01898350.

[54] J. Martinsson Bonde. Multidisciplinary analysis client, June 2022. URL https://doi.org/10.5281/zenodo.6784247.

[55] K. Al Handawi. The margin value method library, 2022. URL https://sed-group.github.io/mvmlib/. Visited 2022-08-09.

[56] K. Al Handawi. Welcome to mvm_paper: the code repository for the design space exploration paper, 2022. URL https://github.com/khbalhandawi/mvm_paper. Visited 2022-08-09.

Accepted Manuscript Not Copyedited

Downloaded from http://asmedigitalcollection.asme.org/mechanicaldesign/article-pdf/doi/10.1115/1.4063966/7056417/md-23-1056.pdf by McGill University user on 06 November 2023

Journal of Mechanical Design. Received February 01, 2023; Accepted manuscript posted October 21, 2023. doi:10.1115/1.4063966
Copyright © 2023 by ASME

Supplemental Material: Design space exploration and evaluation using margin based trade-offs

This appendix clarifies how MVM is used in a Monte-Carlo design simulation in this paper. To ensure the presented algorithm is comprehensible, the basis of the MVM is first briefly described. For further detail on the MVM see ref. [12].

S.I The margin value method by Brahma and Wynn

1. Construct a Margin Analysis Network: The network identifies the flow of information from the input (specification) parameters through decisions to the performance parameters. For some companies, such relationship networks may already exist for a design, which can be reused or adapted to be used in MVM. The following steps describe how to create a MAN:
   (a) Model the design process: The aim of this step is to identify the objectives of the design which are quantified using several performance parameters ($\mathbf{p} \in \mathbb{R}^{n_{\text{perfs}}}$) of interest. The performance of a design is governed by the input specifications ($\mathbf{s} \in \mathbb{R}^{n_{\text{specs}}}_{>0}$) (which must remain strictly positive) and the individual tasks/subtasks that translate inputs to performance parameters. If input specifications are expected to take on zero values, a variable transformation can be used to ensure positivity.
   (b) Identify steps and parameters: For each task/subtask, the individual inputs, outputs, decisions and calculations are identified.
   (c) Connect key parameters into a network: Only the parameters relevant to the calculation of the performance parameters are kept. Inputs and outputs of tasks are connected to each other for all the tasks/subtasks to form a network.
   (d) Construct MAN: Once the network is formed, the margin analysis network can be created by modeling the calculations and decisions involved in each task/subtask. The decisions involve off-the-shelf components, i.e., choosing from a discrete set $\mathcal{D}$ (e.g., the decision for a material $d \in \{\text{Inconel 718, Titanium}\} \in \mathcal{D}$). These decisions involve design margins which are represented using margin nodes. The number of margin nodes is denoted by n. Decisions can be made at the designer's discretion or by minimizing the total excess margin. The MAN can be mathematically expressed as a collection of the following functions which represent the behaviour models.
      i. $\mathbf{f} : \mathbb{R}^{n_{\text{specs}}} \times \mathcal{D} \to \mathbb{R}^n$ is a function that takes input specifications $\mathbf{s}$ and decisions $\mathbf{d}$ as its arguments and returns the corresponding target thresholds $\mathbf{e}^t$.
      ii. The function $\mathbf{g} : \mathcal{D} \to \mathbb{R}^n$ takes decisions $\mathbf{d}$ as its arguments and returns the corresponding decided values $\mathbf{e}^d$.
      iii. The function $\mathbf{h} : \mathbb{R}^{n_{\text{specs}}} \times \mathcal{D} \to \mathbb{R}^{n_{\text{perfs}}}$ takes input specifications $\mathbf{s}$ and decisions $\mathbf{d}$ as its arguments and returns the corresponding performance parameters $\mathbf{p}$.
      iv. The function $\mathbf{g}^{-1}$ takes decided values $\mathbf{e}^d$ as its arguments and returns the corresponding threshold design $\mathbf{d}^{\text{threshold}}$.
2. Margin Value Analysis: The margin value analysis consists of calculating three metrics:
   (a) Local excess margin: Each decision in the margin analysis network is accompanied by excess margin due to a discrepancy between the capability of the of the system/subsystem (defined as the decided value) and what it is required of it to achieve its function (defined as the target threshold). This excess is defined at a margin node belonging to the margin analysis network and is based on Eckert et al.'s definition of excess [2].

$$\mathbf{e} = (\mathbf{f}(\mathbf{s},\mathbf{d}) - \mathbf{g}(\mathbf{d}))\,\mathbf{i}^{\text{excess}\mathsf{T}} = \left(\mathbf{e}^t - \mathbf{e}^d\right)\mathbf{i}^{\text{excess}\mathsf{T}}, \tag{S.1}$$

   where $\mathbf{i}^{\text{excess}}$ is the vector of signs for each margin node. Its components are defined as

$$i^{\text{excess}} = \begin{cases} 1 & \text{if } e^t \text{ must exceed } e^d \\ -1 & \text{if } e^t \text{ must not exceed } e^d \end{cases}. \tag{S.2}$$

   (b) Impact on performance (IoP): The second metric is calculated based on the performance parameters – considering the actual design versus the performance parameters – if it is assumed that the margin is eliminated at each node. Elimination of the ith margin can be done by substituting a vector $\mathbf{e}^d_i$ of decided values, where the ith component e^d_i is set equal to the ith threshold value e^t_i, into $\mathbf{g}^{-1}$ to obtain the *threshold design* $\mathbf{d}^{\text{threshold}}_i = \mathbf{g}^{-1}(e^t_i, e^d_{\neq i})$. The impact may then be calculated by calculating the relative difference in performance between each threshold design

Accepted Manuscript Not Copyedited
Downloaded from http://asmedigitalcollection.asme.org/mechanicaldesign/article-pdf/doi/10.1115/1.4063966/7056417/md-23-1056.pdf by McGill University user on 06 November 2023

Journal of Mechanical Design. Received February 01, 2023;
Accepted manuscript posted October 21, 2023. doi:10.1115/1.4063966
Copyright © 2023 by ASME

and the nominal chosen design.

$$
\begin{aligned}
I_{i,j} &= \frac{h_j(\mathbf{s},\mathbf{d}) - h_j(\mathbf{s},\mathbf{d}_i^{\text{threshold}})}{h_j(\mathbf{s},\mathbf{d}_i^{\text{threshold}})} i_j^p \\
&= \frac{p_j - p_{j,i}^{\text{threshold}}}{p_{j,i}^{\text{threshold}}} i_j^p,
\end{aligned}
\tag{S.3}
$$

where p_j is the jth performance parameter, $p_{j,i}^{\text{threshold}}$ is the jth performance parameter of the ith threshold design, and $\mathbf{i}^p$ is sign of each performance parameter.

$$
i^p = \begin{cases} 1 & \text{if increasing } p \text{ is valuable} \\ -1 & \text{if decreasing } p \text{ is valuable} \end{cases}.
\tag{S.4}
$$

This metric indicates the deteriorating effect of each margin node on each performance parameter. Equation S.3 describes a matrix with dimensions $\mathbf{I} \in \mathbb{R}^{n \times n_{\text{perfs}}}$.

(c) Change absorption capability (CAC): The third metric is calculated by first calculating the variance in the specification possible which do not lead to any changes in the design and then quantifying the effect of that on the margin node. In other words, how much of the margin at each margin node can actually be absorbed without causing a propagation of changes. The allowable variance in the specifications is calculated as follows:

$$
v_k = \frac{s_k^{\max} - s_k}{s_k} i_j^s,
\tag{S.5}
$$

where $s_k^{\max}$ is the value of the kth specification (while setting all others to their nominal values) when any margin $\mathbf{e}$ is less than or equal to zero. We call this value the maximum supported specification. Equation (S.5) is defined because $s_k^{\max}$ and s_k are strictly positive. $\mathbf{i}^s$ is the sign of the expected change in each specification parameter.

$$
i^s = \begin{cases} 1 & s \text{ is expected to increase} \\ -1 & s \text{ is expected to decrease} \end{cases}.
\tag{S.6}
$$

This value is found by iterating each specification until $\mathbf{e} < 0$. The next step is to calculate the portion of absorbed margin for each specification by calculating the relative change in the threshold values.

$$
\begin{aligned}
A_{i,k} &= \frac{f_i(s_k^{\max}, s_{\neq k}, \mathbf{d}) - f_i(\mathbf{s},\mathbf{d})}{f_i(\mathbf{s},\mathbf{d}) v_k} \\
&= \frac{e_{k,i}^{t,\max} - e_i^t}{e_i^t v_k},
\end{aligned}
\tag{S.7}
$$

where e_i^t is the ith threshold parameter, $e_{k,i}^{t,\max}$ is the ith threshold parameter corresponding to the kth maximum supported specification. Equation S.7 describes a matrix with dimensions $\mathbf{A} \in \mathbb{R}^{n \times n_{\text{specs}}}$.

3. Aggregating metrics: The method suggests that the metrics calculated for impact and absorption be averaged based on the relative importance of the the performance parameters and the prioritisation of change in the specification. This leads to aggregate values of the two metrics. In this paper, we assume equal weightings for all performance parameters and input specifications. The aggregation can be performed by averaging the impact on each performance parameter

Accepted Manuscript Not Copyedited

Downloaded from http://asmedigitalcollection.asme.org/mechanicaldesign/article-pdf/doi/10.1115/1.4063966/7056417/md-23-1056.pdf by McGill University user on 06 November 2023

Journal of Mechanical Design. Received February 01, 2023;
Accepted manuscript posted October 21, 2023. doi:10.1115/1.4063966
Copyright © 2023 by ASME

and absorption capability for each input specification for margin node i.

$$\bar{A}_i = \frac{1}{n_{\text{specs}}} \sum_{k=1}^{n_{\text{specs}}} A_{i,k}$$
$$\bar{I}_i = \frac{1}{n_{\text{perfs}}} \sum_{j=1}^{n_{\text{perfs}}} I_{i,j} \tag{S.8}$$

4. Margin Value Plot: The two metrics ($\bar{\mathbf{A}}$ and $\bar{\mathbf{I}}$) can then be plotted which shows the relative importance of the ith margin node in terms of their absorption capability and the deteriorating effect on the performance of the system.

Algorithm 1 shows the implementation of the MVM in this paper and its corresponding library `mvmlib` [3].

Accepted Manuscript Not Copyedited

Downloaded from http://asmedigitalcollection.asme.org/mechanicaldesign/article-pdf/doi/10.1115/1.4063966/7056417/md-23-1056.pdf by McGill University user on 06 November 2023

Journal of Mechanical Design. Received February 01, 2023; Accepted manuscript posted October 21, 2023. doi:10.1115/1.4063966
Copyright © 2023 by ASME

Algorithm 1: Pseudo-algorithm for the margin value method (MVM)

Input: set of possible choices $\mathcal{D}$, chosen design $\mathbf{d} \in \mathcal{D}$
sign of excess $\mathbf{i}^{\text{excess}}$, sign of performance parameters $\mathbf{i}^p$, sign of input specifications $\mathbf{i}^s$, Rate of change of input specifications $\mathbf{\Delta}^s$, the MAN given by $\mathbf{f}, \mathbf{g}, \mathbf{h},$ and $\mathbf{g}^{-1}$, n_{samples}, and Joint PDF $F_{\mathbf{S}}(\mathbf{s})$ for modeling uncertain specifications.

Output: expected impact on performance and change absorption capability $\bar{\bar{\mathbf{I}}}$, $\bar{\bar{\mathbf{A}}}$

[0] Initialization

set counter $i_{\text{sample}} \leftarrow 0$, initialize expected impact and absorption $\bar{\bar{\mathbf{I}}} \in \mathbb{R}^n$ and $\bar{\bar{\mathbf{A}}} \in \mathbb{R}^n$

[1] Monte-carlo simulation

draw sample input specifications $\mathbf{S} \in \mathbb{R}^n \sim F_{\mathbf{S}}(\mathbf{s})$

[2] Calculate threshold, decided, excess, and performance values

$\mathbf{e}^t = \mathbf{f}(\mathbf{S}, \mathbf{d})$

$\mathbf{e}^d = \mathbf{g}(\mathbf{d})$

$\mathbf{e} = \left(\mathbf{e}^t - \mathbf{e}^d\right) \mathbf{i}^{\text{excess}\mathsf{T}}$

$\mathbf{p} = \mathbf{h}(\mathbf{S}, \mathbf{d})$

[3] Check feasibility

if $\exists\, i$ such that $e_i < 0$ **then** set $i_{\text{sample}} \leftarrow i_{\text{sample}} + 1$ go to **[1]**

else go to **[4]**

[4] Calculate allowable deterioration

initialize vector of maximum supported specifications $\mathbf{s}^{\max} \in \mathbb{R}^{n_{\text{specs}}}$

loop over input specifications **for** $k = 1, 2, \ldots, n_{\text{specs}}$ **do**

  Solve $\min \left(\mathbf{f}(\hat{s}_k, s_{\neq k}, \mathbf{d}) - \mathbf{g}(\mathbf{d})\right) \mathbf{i}^{\text{excess}\mathsf{T}}$ for $\hat{s}_k$ **while** residual $< \mathbf{0}$ **do**

    $\hat{s}_k \leftarrow \hat{s}_k + i_k^s \Delta_k^s$

  $s_k^{\max} \leftarrow \hat{s}_k$

[5] Calculate margin value metrics

initialize impact and absorption matrices

$\mathbf{I} \in \mathbb{R}^{n_{\text{perfs}} \times n} \leftarrow \mathbf{0}$ and $\mathbf{A} \in \mathbb{R}^{n_{\text{specs}} \times n} \leftarrow \mathbf{0}$

initialize deterioration, IoP, and CAC vectors

$\mathbf{v} \in \mathbb{R}^{n_{\text{specs}}} \leftarrow \mathbf{0}$, $\bar{\mathbf{I}} \in \mathbb{R}^n \leftarrow \mathbf{0}$, and $\bar{\mathbf{A}} \in \mathbb{R}^n \leftarrow \mathbf{0}$

loop over margin nodes **for** $i = 1, 2, \ldots, n$ **do**

  [a] Calculate impact on performance

  $\mathbf{d}_i^{\text{threshold}} = \mathbf{g}^{-1}(e_i^t, e_{\neq i}^d)$

  $\mathbf{p}_i^{\text{threshold}} = \mathbf{h}(\mathbf{S}, \mathbf{d}_i^{\text{threshold}})$

  loop over performance parameters **for** $j = 1, 2, \ldots, n_{\text{perfs}}$ **do**

    $I_{i,j} \leftarrow \dfrac{p_j - p_{j,i}^{\text{threshold}}}{p_{j,i}^{\text{threshold}}} i_j^p$

  [b] Calculate change absorption capability

  loop over input specifications **for** $k = 1, 2, \ldots, n_{\text{specs}}$ **do**

    calculate deterioration $v_k \leftarrow \dfrac{s_k^{\max} - s_k}{s_k} i_k^s$

    $A_{i,k} \leftarrow \dfrac{f_i(s_k^{\max}, s_{\neq k}, \mathbf{d}) - f_i(\mathbf{s}, \mathbf{d})}{f_i(\mathbf{s}, \mathbf{d}) v_k}$

  [c] Aggregate metrics

  $\bar{A}_i \leftarrow \text{mean}\,(A_i)\ \forall\, A_{i,k} \neq 0$

  $\bar{I}_i \leftarrow \text{mean}\,(I_i)\ \forall\, I_{i,j} \neq 0$

[6] sum of Monte Carlo samples

$\bar{\bar{\mathbf{A}}} \leftarrow \bar{\bar{\mathbf{A}}} + \bar{\mathbf{A}}$

$\bar{\bar{\mathbf{I}}} \leftarrow \bar{\bar{\mathbf{I}}} + \bar{\mathbf{I}}$

[7] Termination

if $i_{sample} < n_{samples}$ **then** $i_{\text{sample}} \leftarrow i_{\text{sample}} + 1$

go to **[1]**

else $\bar{\bar{\mathbf{A}}} \leftarrow \bar{\bar{\mathbf{A}}}/n_{\text{samples}}$ and $\bar{\bar{\mathbf{I}}} \leftarrow \bar{\bar{\mathbf{I}}}/n_{\text{samples}}$

stop

Accepted Manuscript Not Copyedited

Downloaded from http://asmedigitalcollection.asme.org/mechanicaldesign/article-pdf/doi/10.1115/1.4063966/7056417/md-23-1056.pdf by McGill University user on 06 November 2023

Journal of Mechanical Design. Received February 01, 2023;
Accepted manuscript posted October 21, 2023. doi:10.1115/1.4063966
Copyright © 2023 by ASME

S.II The turbine rear structure

Figure S.I below shows the exact location of the TRS within an aeroengine.

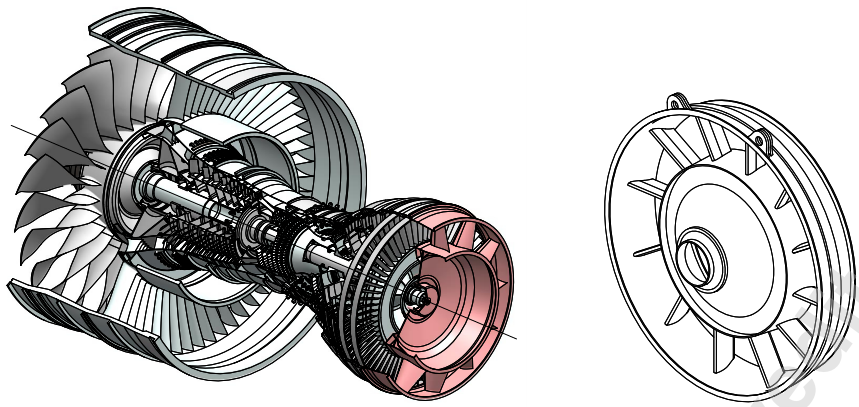

(a) (b)

Fig. S.I: (a) CAD model of a turbofan engine with the TRS highlighted in red. (b) computer-aided design model of the TRS.

S.III Strut preliminary analysis model

Figure S.II shows the different loads that the strut should support under thermal loading. We describe a parametric model for the analysis and design of a single strut under thermal loading. We assume that the same calculations apply to all struts due to cyclic symmetry of the TRS. We also ignore fracture as a possible failure mode because it would unnecessarily complicate the analysis in this paper with regards to its objectives. Fracture has been modeled and studied as part of previous research [4].

We show a simplified sector of the TRS in Figures S.IIa and S.IIb. The first illustration shows how the lean angle of the strut can be used to calculate its length using geometry. The second illustration shows the effect of thermal loading on the strut and its resulting expansion. Thermal loads arise due to a temperature gradient across the strut. The inner hub experiences a temperature T_1 that is greater than the shroud temperature T_2 resulting in compressive loading on the strut. The net deflection of the strut $\delta_2 - \delta_1$ results in axial and bending loads on the strut as shown in Figure S.IIb. The first calculation pertains to the length L of the strut in terms of the lean angle θ. Equation (S.9) gives the expression that relates L to θ.

$$L = -r_1 \cos\theta + \sqrt{{r_2}^2 - {r_1}^2 \sin^2\theta}. \tag{S.9}$$

We calculate the axial force F, axial stress σ_a, and bending stress σ_m as given by Equation (S.10).

$$\begin{aligned} F &= \frac{Ewh\alpha}{L}\left(T_2 r_2 - T_1 r_1 - T_{\text{sink}}(r_2 - r_1)\right)\cos\theta \\ \sigma_a &= \frac{E\alpha}{L}\left(T_2 r_2 - T_1 r_1 - T_{\text{sink}}(r_2 - r_1)\right)\cos\theta \\ \sigma_m &= \frac{3}{2}\frac{Eh\alpha}{L^2}\left(T_2 r_2 - T_1 r_1 - T_{\text{sink}}(r_2 - r_1)\right)\sin\theta, \end{aligned} \tag{S.10}$$

where E is the elastic modulus, α is the coefficient of thermal expansion, and T_{sink} is the ambient temperature which are all treated as constants for simplicity. The maximum buckling load that can sustained by the strut is calculated using the Euler-buckling equation in terms of the effective length factor $K = 1.0$ for a pinned-pinned beam in Equation (S.11).

$$F_{\text{buckling}} = \frac{\pi^2 EI}{(KL)^2} = \frac{\pi^2 Ewh^3}{12\,(KL)^2}. \tag{S.11}$$

Accepted Manuscript Not Copyedited

Downloaded from http://asmedigitalcollection.asme.org/mechanicaldesign/article-pdf/doi/10.1115/1.4063966/7056417/md-23-1056.pdf by McGill University user on 06 November 2023

Journal of Mechanical Design. Received February 01, 2023;
Accepted manuscript posted October 21, 2023. doi:10.1115/1.4063966
Copyright © 2023 by ASME

The final step is to calculate the weight and raw material cost of the strut simply given by Equation (S.12).

$$\begin{aligned} W &= \rho whL \\ c_{\text{raw}} &= c\rho whL, \end{aligned} \tag{S.12}$$

where ρ and c are the chosen material's weight and cost densities, respectively. The second loadcase involves two additional input specifications corresponding to a load on the bearing as shown in Figure 2d. A simulation model is used to assess the load carrying capacity of the TRS under static bearing loads and return the required number of struts n_{struts}.

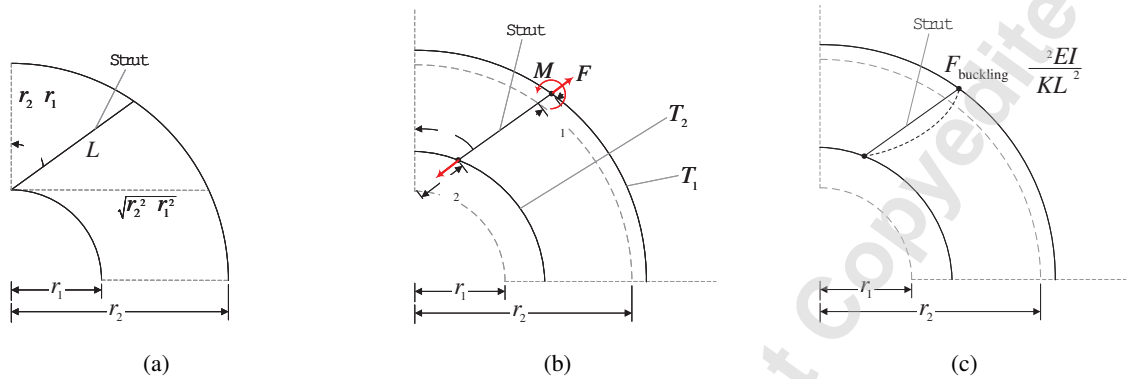

Fig. S.II: (a) Geometric model, (b) thermal expansion model, and (c) calculation of the buckling load on a leaned strut.

The models described earlier are summarized in Table S.I below in the context of the MAN for polygonal shroud concepts in Figure S.III. The vector of excess signs is defined as $\mathbf{i}^{\text{excess}} = [-1\ -1\ -1]^{\mathsf{T}}$ since the target threshold must

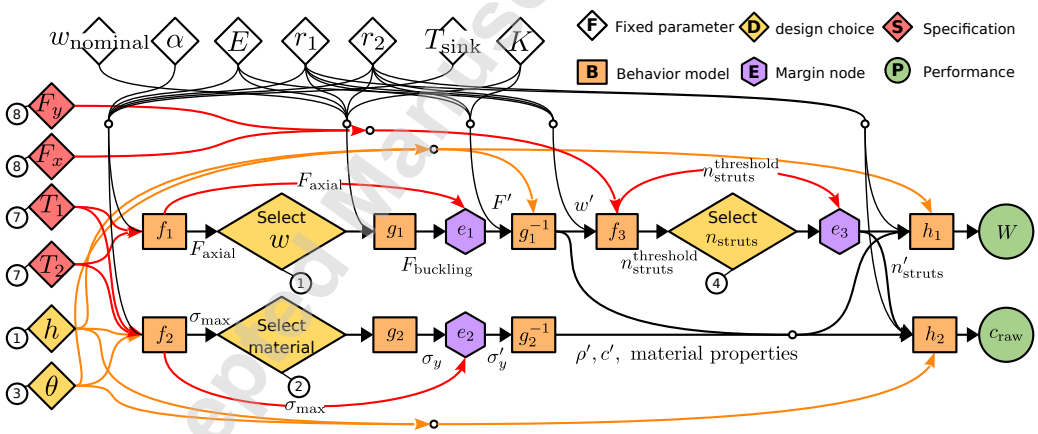

Fig. S.III: MAN for performing margin analysis on concepts with polygonal shrouds. The small numbered circles are hyperlinks showing how nodes on the margin network relate to particular functions and means in the EF-M given by Figure 3.

not exceed the decided value for all margin nodes. The vector of performance signs is $\mathbf{i}^p = [-1\ -1]^{\mathsf{T}}$ since decreasing both performance parameters is valuable. The vector of input specification signs is $\mathbf{i}^s = [1\ -1\ 1\ 1]^{\mathsf{T}}$ since all input specifications are expected to increase except for the shroud temperature T_2. d_1,d_2, and d_3 are chosen such that the excess values e_1, e_2, e_3 are minimized by computing their values using Equation (S.1) and minmizing over the possible choices $\mathcal{D}$.

$$\underset{\mathbf{d}\in\mathcal{D}}{\text{minimize}} \quad \mathbf{e}(\mathbf{S}, d) = (\mathbf{f}(\mathbf{S}, \mathbf{d}) - \mathbf{g}(\mathbf{d}))\,\mathbf{i}^{\text{excess}\,\mathsf{T}}. \tag{S.13}$$

Accepted Manuscript Not Copyedited

Downloaded from http://asmedigitalcollection.asme.org/mechanicaldesign/article-pdf/doi/10.1115/1.4063966/7056417/md-23-1056.pdf by McGill University user on 06 November 2023

Journal of Mechanical Design. Received February 01, 2023;
Accepted manuscript posted October 21, 2023. doi:10.1115/1.4063966
Copyright © 2023 by ASME

Table S.I: Definitions of behaviour models, that are shown as orange boxes in Figure S.III. Also see explanations in the supplemental material Section S.III.

Function	Inputs	Outputs	Description
f_1	T_1, T_2, h, θ, α, E, r_1, r_2, T_{sink}	F_{axial}	$F = Ewh\alpha(T_2r_2 - T_1r_1 - T_{\text{sink}}(r_2 - r_1))\cos\theta/L$
f_2	T_1, T_2, h, θ, α, E, r_1, r_2, T_{sink}	$\sigma_{\max}$	$\max\begin{pmatrix}\sigma_a = E\alpha(T_2r_2 - T_1r_1 - T_{\text{sink}}(r_2 - r_1))\cos\theta/L \\ \sigma_m = \frac{3}{2}\frac{Eh\alpha}{L^2}(T_2r_2 - T_1r_1 - T_{\text{sink}}(r_2 - r_1))\sin\theta\end{pmatrix}$
f_3	σ'_y, w', h, θ, B_X, B_Y, E, r_1, r_2	$n_{\text{struts}}^{threshold}$	Polynomial fit from simulation
g_1	w_{nominal}, h, θ, E, r_1, r_2, K	F_{buckling}	$F_{\text{buckling}} = \frac{\pi^2 E w_{\text{nominal}} h^3}{12(KL)^2}$
g_2	material	σ_y, ρ, c	Lookup table of material properties
h_1	ρ', w', n'_{struts}, h, θ, r_1, r_2	W	$W = \rho whLn_{\text{struts}}$
h_2	ρ', c', w', n'_{struts}, h, θ, r_1, r_2	c_{raw}	$c_{\text{raw}} = c\rho whLn_{\text{struts}}$
g_1^{-1}	$F', h, \theta, E, r_1, r_2, K$	w'	$w' = \frac{12(KL)^2 F'}{\pi^2 Ewh^3}$
g_2^{-1}	σ'_y	ρ', c'	Interpolation of material lookup table

Note: $L = -r_1\cos\theta + \sqrt{{r_2}^2 - {r_1}^2\sin^2\theta}$. Also see Figure 2b

Table S.II: EF-M independent parameters of the MAN for polygonal shroud (see Figure S.III).

Symbol	Units	Description
Fixed parameters		
E	GPa	Young's modulus
α	$^{\circ}\text{C}^{-1}$	Thermal expansion coefficient
r_1	mm	Radius of the hub
r_2	mm	Radius of the shroud
K		Column effective length factor
T_{sink}	$^{\circ}$C	Ambient temperature
w_{nominal}	mm	nominal buckling width
Intermediate parameters		
σ'_y	MPa	yield strength
F'	N	axial load
w'	mm	cross-section (vane) width
n'_{struts}		number of struts
ρ'	kg/mm^3	density
c'	\$/mm^3	cost density
Performance parameters		
W	kg	Weight of the strut
c_{raw}	\$	Raw material cost
Target thresholds		
Node / **Symbol**	**Units**	**Description**
e_1 / F_{axial}	N	Compressive force on strut
e_2 / $\sigma_{\max}$	MPa	Maximum stress on strut
e_3 / $n_{\text{struts}}^{\text{threshold}}$	MPa	Required number of struts
Decided values		
e_1 / F_{buckling}	N	Buckling load of strut
e_2 / σ_y	MPa	Yield stress
e_3 / n_{struts}	MPa	Number of struts

S.IV Shroud preliminary analysis model

We consider the design of the shroud of the TRS from a static loading point view. We consider the worst-case scenario, where the resolved bearing load B is applied directly through one of the struts as given by Equation (S.14).

$$B = \sqrt{B_x^2 + B_y^2}. \tag{S.14}$$

Accepted Manuscript Not Copyedited

Downloaded from http://asmedigitalcollection.asme.org/mechanicaldesign/article-pdf/doi/10.1115/1.4063966/7056417/md-23-1056.pdf by McGill University user on 06 November 2023

Journal of Mechanical Design. Received December 2022.
Accepted manuscript posted October 21, 2023. doi:10.1115/1.4063966
Copyright © 2023 by ASME

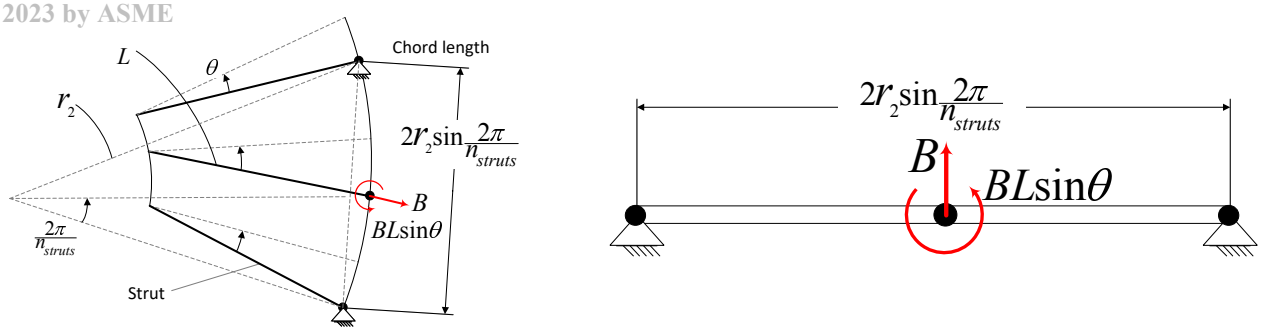

(a) (b)

Fig. S.IV: (a) Application of bearing load B to shroud and (b) simplified beam model of a shroud section.

The adjacent struts would act as fixed supports resulting in a bending load on the shroud as shown in Figure S.IVab. The curvature of the shroud can be ignored since the chord length spanned by two struts is small compared to the shroud radius $2r_2 \sin \frac{2\pi}{n_{\text{struts}}} \ll r_2$. The maximum bending stress on the shroud would be given by the following expression

$$\sigma_s = \frac{6B}{w_s {t_s}^2}\left(L\sin\theta + r_2 \sin\frac{2\pi}{n_{\text{struts}}}\right). \tag{S.15}$$

Finally, the weight of the shroud can calculated as a function the shroud width w_s such that it is given by the volumn of a hollow cylinder as follows

$$W_{\text{shroud}} = \rho_s \pi w_s t_s \left(2r_2 + t_s\right). \tag{S.16}$$

The vector of excess signs for circumferential shroud concepts is defined as $\mathbf{i}^{\text{excess}} = [-1\ -1\ -1\ -1]^{\mathsf{T}}$ since the target threshold must not exceed the decided value for all four margin nodes. The vector of performance signs is $\mathbf{i}^{p} = [-1\ -1\ -1\ -1]^{\mathsf{T}}$ since decreasing all performance parameters is valuable. The vector of input specification signs is just as before in Section S.III, i.e., $\mathbf{i}^{s} = [1\ -1\ 1\ 1]^{\mathsf{T}}$.

S.V Margin analysis network of concepts with circumferential shrouds

Based on the previous analysis of the struts and shrouds in Sections S.III and S.IV, we can construct a MAN for alternatives TRSs with circumferential shrouds as shown in Figure 4. The shroud design is only considered as part of the circumferential shroud configuration (and not the polygonal shrouds) since, such shrouds provide less stiffness against structural loads and are more susceptible to static failure. These added considerations, result in an additional margin node e_4, and two additional performance parameters (W_s and c_s). Input specifications (red diamonds) and design decisions (orange diamonds) which interact with the EF-M are defined in Table 2. Fixed (white diamonds), intermediate, and performance parameters (green circles) which do not interact with the EF-M directly are defined in Table 3. All the behaviour models (orange boxes) are defined in Table S.III, where the length of the strut is given at the bottom of the table.

Accepted Manuscript Not Copyedited

Downloaded from http://asmedigitalcollection.asme.org/mechanicaldesign/article-pdf/doi/10.1115/1.4063966/7056417/md-23-1056.pdf by McGill University user on 06 November 2023

Journal of Mechanical Design. Received December 2022.
Accepted manuscript posted October 21, 2023. doi:10.1115/1.4063966
Copyright © 2023 by ASME

Table S.III: Definitions of behaviour models, that are shown as orange boxes in Figure 4b.

Function	Inputs	Outputs	Description
f_1	T_1, T_2, h, θ, α, E, r_1, r_2, T_{sink}	F_{axial}	$F = Ewh\alpha\left(T_2 r_2 - T_1 r_1 - T_{\text{sink}}(r_2 - r_1)\right)\cos\theta/L$
f_2	T_1, T_2, h, θ, α, E, r_1, r_2, T_{sink}	$\sigma_{\max}$	$\max\begin{pmatrix}\sigma_a = E\alpha\left(T_2 r_2 - T_1 r_1 - T_{\text{sink}}(r_2 - r_1)\right)\cos\theta/L \\ \sigma_m = \frac{3}{2}\frac{Eh\alpha}{L^2}\left(T_2 r_2 - T_1 r_1 - T_{\text{sink}}(r_2 - r_1)\right)\sin\theta\end{pmatrix}$
f_3	σ'_y, w', h, θ, B_X, B_Y, E, r_1, r_2	$n^{threshold}_{\text{struts}}$	Polynomial fit from simulation
f_4	B_x, B_y	B	$B = \sqrt{B_x^2 + B_y^2}$
g_1	w_{nominal}, h, θ, E, r_1, r_2, K	F_{buckling}	$F_{\text{buckling}} = \frac{\pi^2 E w_{\text{nominal}} h^3}{12\,(KL)^2}$
g_2	material	σ_y, ρ, c	Lookup table of material properties
g_3	σ'_y, n'_{struts}, t_s, θ, r_1, r_2, w_s	$B_{\max}$	$B_{\max} = \frac{\sigma'_y w_s t_s^2}{6\left(L\sin\theta + r_2 \sin\frac{2\pi}{n'_{\text{struts}}}\right)}$
h_1	ρ', w', n'_{struts}, h, θ, r_1, r_2	W	$W = \rho' w' h L n'_{\text{struts}}$
h_2	ρ', c', w', n'_{struts}, h, θ, r_1, r_2	c_{raw}	$c_{\text{raw}} = c'\rho' w' h L n'_{\text{struts}}$
h_3	ρ', t'_s, r_2, w_s	W_s	$W_s = \rho'\pi t'_s\left(t'_s + 2r_2\right) w_s$
h_4	ρ', c', t'_s, r_2, w_s	c_s	$c_s = c'\rho'\pi t'_s\left(t'_s + 2r_2\right) w_s$
g_1^{-1}	F', h, θ, E, r_1, r_2, K	w'	$w' = \frac{12\,(KL)^2 F'}{\pi^2 E w h^3}$
g_2^{-1}	σ'_y	ρ', c'	Interpolation of material lookup table
g_3^{-1}	B', σ'_y, n'_{struts}, θ, r_1, r_2, w_s	t'_s	$t'_s = \sqrt{\frac{6B'}{w_s \sigma'_y}\left(L\sin\theta + r_2\sin\frac{2\pi}{n'_{\text{struts}}}\right)}$

Note: $L = -r_1\cos\theta + \sqrt{{r_2}^2 - {r_1}^2\sin^2\theta}$. Also see Figure 2b

Accepted Manuscript Not Copyedited

Downloaded from http://asmedigitalcollection.asme.org/mechanicaldesign/article-pdf/doi/10.1115/1.4063966/7056417/md-23-1056.pdf by McGill University user on 06 November 2023

Journal of Mechanical Design. Received February 01, 2023;
Accepted manuscript posted October 21, 2023. doi:10.1115/1.4063966
Copyright © 2023 by ASME

S.VI Supporting results

The plot below shows the cumulative marginal distribution of the CAC and IoP of margin node $e3$ of concept A ($h = 15$ mm $\theta = 0^o$) of the limited example described at the beginning of Section 4. The variation arises due to variance in the input specifications T_1, T_2, B_x, and B_y which are also shown on the same plot. The plot also shows the breakdown of the decisions taken for each input specification sample given by the color codes. The most frequent decision (shown in green) is to use 12 70 mm Inconel struts for the decisions of the MAN as it can accommodate a wide range of input specifications.

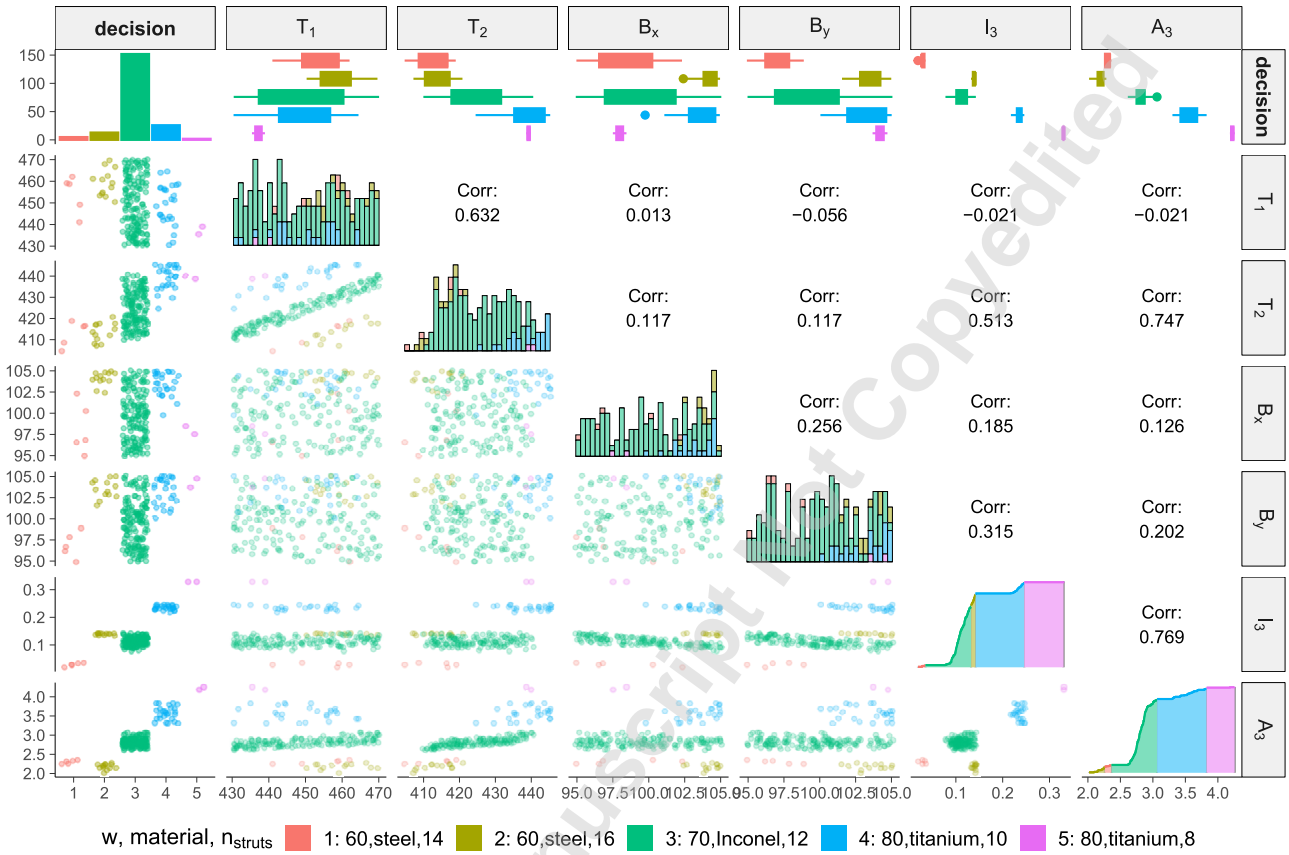

Fig. S.V: Scatter plot matrix of IoP and CAC of margin node e_3 of the conceptual alternative $\theta = 0^o$, and $h = 15$ mm. The plot shows the distribution of input specifications, IoP, and CAC binned by the decisions taken for each input specifications sample. The diagonal plots for the input specifications T_1, T_2, B_x, and B_y represent their marginal frequency distributions while those of the IoP I_3 and CAC A_3 represent the marginal cumulative frequency distribution. The off-diagonal plots represent the correlation plots between the marginal frequency distributions for each element. The variation arises from the variation in input specifications.

Accepted Manuscript Not Copyedited

Downloaded from http://asmedigitalcollection.asme.org/mechanicaldesign/article-pdf/doi/10.1115/1.4063966/7056417/md-23-1056.pdf by McGill University user on 06 November 2023

References

[1] A. Brahma, D. Wynn. Margin value method for engineering design improvement. *Research in Engineering Design*, 31(3), 353–381, 2020. https://doi.org/10.1007/s00163-020-00335-8

[2] C. Eckert, O. Isaksson, C. Earl. Design margins: A hidden issue in industry. *Design Science*, 5, e9, 2019. https://doi.org/10.1017/dsj.2019.7

[3] mvmlib. The margin value method library. 2021. [Online]. Available: https://sed-group.github.io/mvmlib/

[4] K. Al Handawi, P. Andersson, M. Panarotto, O. Isaksson, M. Kokkolaras. Scalable set-based design optimization and remanufacturing for meeting changing requirements. *Journal of Mechanical Design*, 143(2), 2020. https://doi.org/10.1115/1.4047908